International Journal of Plasticity 155 (2022) 103320

Contents lists available at ScienceDirect

International Journal of Plasticity

journal homepage: www.elsevier.com/locate/ijplas

Revealing the influential mechanism of strain ranges on cyclic-life saturation during creep-fatigue in Nickel-based superalloy DZ445

Biao Ding [a], Weili Ren [a,*], Yunbo Zhong [a,*], Xiaotan Yuan [a], Tianxiang Zheng [a], Zhe Shen [a,*], Yifeng Guo [a], Qiang Li [a], Jianchao Peng [b], Josip Brnic [c], Yanfei Gao [d], Peter K. Liaw [d]

[a] State Key Laboratory of Advanced Special Steel, College of Materials Science and Engineering, Shanghai University, Shanghai, P.R. China
[b] Laboratory for Microstructures, Shanghai University, Shanghai, P.R. China
[c] University of Rijeka, Faculty of Engineering, Vukovarska 58, Rijeka, Croatia
[d] Department of Materials Science and Engineering, University of Tennessee, Knoxville, USA

ARTICLE INFO

Keywords:
Creep-fatigue
Cyclic-life "saturation phenomenon"
Total strain ranges
Superalloys
Mechanical response
Deformation mechanisms

ABSTRACT

The creep-fatigue interaction has been recognized as the main failure mode of most structural components operating in the high-temperature regime. The cyclic life (N_f) usually decreases continuously with the dwell time in their interactions. However, N_f shows an abnormal change, i.e. keeps constant or slightly increases/decreases, in the present studied Nickel-based superalloy, DZ445. This means that generalized "N_f saturation" is achieved by a dynamic equilibrium between the straight single superdislocations and dislocation networks corresponding to local and homogeneous damage, respectively. The saturation appears more easily with the increasing high strain ranges. The variation in the mechanical response parameters, the damage characterizations, and the phase involutions with the increasing dwell time exhibits the low amplitude under the high strain range. The combined characteristics show that the easy occurrence of N_f saturation in the range of large deformations is obtained by increasing the local-damage. The low change rate of straight single superdislocations with the dwell time in the range of large deformation is well confirmed by the above mechanism. The parameters in the different criterion models of the cyclic-life "saturation phenomenon" unify the mechanical response and the damage mechanism soundly. The work provides a new theoretical basis and guidance for the creep-fatigue safety design of high-temperature metallic materials and the establishment of dislocation-based models.

1. Introduction

It is of great importance to anticipate and prevent the component failure, especially for high-temperature structural materials (Kruzic, 2009). Directionally-solidified (DS) Ni-based superalloys as typical high-temperature materials possess the solid-solution matrix (γ phase) with coherent precipitates (γ′) of the $L1_2$ structure, constituting around 60 - 70% in volume in the microstructure, which offers a unique combination of fatigue, creep, and oxidation resistance (Smith et al., 2016). Although creep resistance is the primary consideration in the design of DS Ni-based superalloys, fatigue performance, particularly with dwell time, i.e. creep-fatigue interactions, is usually a durability concern for service life (Yablinsky et al., 2008). In particular, it could well describe the operation

* Corresponding authors.
E-mail addresses: wlren@staff.shu.edu.cn (W. Ren), yunboz@staff.shu.edu.cn (Y. Zhong), xiabai@shu.edu.cn (Z. Shen).

https://doi.org/10.1016/j.ijplas.2022.103320
Received 22 October 2021; Received in revised form 24 April 2022;
Available online 1 May 2022

during start-up, operation, and shut-down process for turbines and guide blades (Reed, 2006). However, limited by the complexity of experimental equipment and operation, most investigations reported the pure fatigue (León-Cázares et al., 2020a; Liu et al., 2020) and the pure creep behavior (Kim et al., 2016; Wu et al., 2020), but a few on their interactions (Cao et al., 2021; Rodas and Neu, 2018). The purpose of creep-fatigue tests in laboratory is to obtain the fatigue life at the sample level and to simulate the damage distribution in high-temperature structures (Hales, 1980). Therefore, the strain-controlled creep-fatigue experiment under appropriate conditions in laboratory has engineering significance to guide the fatigue life design of component.

The creep-fatigue failure belongs to the category of low-cycle-fatigue deformation according to the division principle of the fatigue life, whose performance is usually evaluated by the cyclic life (N_f) (Zhang and Zhang, 2011). It has been noticed that N_f usually continues to decrease with the dwell time in the creep-fatigue interactions (Hormozi et al., 2015; Porter et al., 2019). However, in rare cases does N_f remain constant or increase/decrease slightly with the dwell time. In 1973, this interesting phenomenon was reported by Conway and the term of "saturation" was first used (Conway et al., 1973). The similar phenomenon was called as N_f "restoration" by Wareing (Wareing, 1981). In superalloy systems, the similar cyclic- life of the DZ125 superalloy at 2 and 5 min dwell times was considered as an abnormal phenomenon (Shi et al., 2010). In the creep-fatigue of GH4169 (Chen et al., 2016) and Incoloy-800H superalloy (Meurer et al., 1984), the reason for N_f "saturation" is not mentioned. In general, according to the recent literature on N_f saturation, some researchers believe that the data are unreliable or that the reason is not mentioned or is simply assumed. The importance of the cyclic-life "saturation phenomenon" in creep-fatigue deformation is just similar to the stress-fatigue limit of the S - N (applied stress – fatigue cycle life) curve in the high-cycle fatigue. When the N_f saturation phenomenon appears, the creep-fatigue test under long-term dwell time can be avoided or greatly reduced. While this vital phenomenon of the "saturation phenomenon" has not received attention since it was proposed. The main factors affecting the creep-fatigue cyclic-life are the total strain range ($\Delta\varepsilon_t$) (Tian et al., 2016), temperature (Takahashi, 2008), environment (Gordon et al., 2006), and loading conditions (Hu et al., 2016). At present, the factors that affected this N_f saturation phenomenon have never been studied in-depth, and the corresponding underlying mechanism has not been revealed. Thus, it naturally follows to analyze the influence factors and the mechanisms lying behind the N_f "saturation phenomenon". This investigation focuses on the influence of strain range about this significant phenomenon.

Combined with our previous creep-fatigue results with 0 - 8 min dwell times at 900 °C and with a total strain range of 1.6% (Ding et al., 2018b), the long dwell times with 16, 32, 64, and 128 min were applied in the present work to verify the existence of the cyclic-life "saturation phenomenon" of creep-fatigue deformation in detail. The results indeed confirm the proposition, which is embodied by the N_f change. It decreases sharply first, followed by slightly decreasing or increasing with the dwell time, which is firstly defined as the generalized "saturation phenomenon". Then, the influence mechanisms of total strain ranges on the N_f "saturation phenomenon" in DZ445 superalloy would be systematically clarified, based on the mechanical response and the damage feature. The larger strain range results in the higher ratio of mobile superdislocations cutting into the γ′ phase, resulting in the greater localized-damage characteristic. It has also been shown that cracks and cavities change from homogeneous to mode of localized deformation with increasing range of deformations. Different models for the cyclic-life "saturation phenomenon" are also finally given to combine these parameters. The greater the inelastic-strain-energy absorption capacity is present in higher strain range. The work provides a new theoretical basis and guidance for the creep-fatigue safety design of high-temperature metallic materials and the establishment of dislocation-based crystal plasticity models.

2. Experimental

2.1. Material preparation

The directionally-solidified Nickel-based superalloy, DZ445, studied in our investigation, consisted of the following ingredients: 0.072 C, 13.10 Cr, 9.99 Co, 4.53 W, 1.75 Mo, 4.07 Al, 2.38 Ti, 4.80 Ta, 0.024 B, and Ni is the balance (weight percent, wt.%). The Bridgeman directional-solidification method with a drawing rate of 7 mm/min was used to produce a rod-shaped superalloy with a size of Φ 16 mm × 210 mm. The heat treatment regime is: 1210 ± 10 °C/2 h/AC + 1080 ± 10 °C/3 h/AC + 850 ± 10 °C/24 h/AC (AC: air

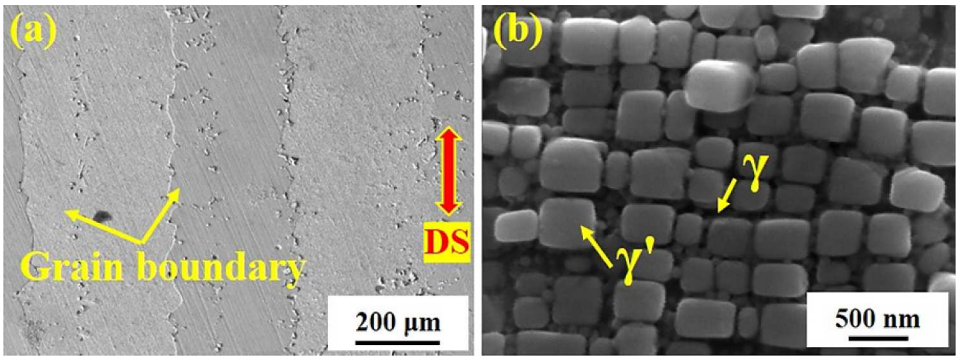

Fig. 1. Grain boundary of the DZ445 superalloy (a); the γ′ precipitate dispersed in the γ matrix channel after the heat treatment (b). (The red arrow and the abbreviation of "DS" represent the direction of the solidification.).

cooling). The creep-fatigue specimen size is Φ 8.5 mm x 101.6 mm where gage length was 26 mm. Fig. 1(a) shows that the columnar grain boundary arranged in parallel. Fig. 1(b) shows the typical coarse cubic γ′ precipitate with the average size of about 350 nm after heat treatment. They are separated in the γ matrix channel with the average width of about 80 nm. Other detailed microstructures of this superalloy before and after heat treatment were shown in our previous study (Ding et al., 2018a).

2.2. Low-cycle-fatigue and creep-fatigue tests

All the strain-controlled creep-fatigue experiments with different total strain ranges were carried out on RPL100 electronic creep-fatigue testing machines. The constant rate of strain loading/unloading is $5 \times 10^{-3}\ s^{-1}$ with or without the dwell time. The different dwell times were introduced at the maximum tensile strain to form a trapezoidal wave. The strain ratio, R ($R = \varepsilon_{\min} / \varepsilon_{\max}$) is −1. Three K-type thermocouples were used to monitor the temperature of the sample. During the tests, the temperature change along the gage length is within ± 2 °C. The rail-type high-temperature extensometer was used to control the total strain range. All the creep-fatigue experimental parameters are shown in Table 1. The experiment was carried out until the sample was fractured. Each experiment under the prescribed test condition was repeated 2 - 3 times.

2.3. Characterization

The morphologies of fracture, lateral cracks, and internal voids for fractured samples were observed by scanning electron microscopy (SEM). Ten SEM images with the same magnification below the fracture along both sides of longitudinal fracture were taken to count the distribution of lengths and opening-angles for the lateral cracks. The lengths and opening angles of these cracks are defined as from the surface crack-initiation to crack-termination point, and by the crack-termination point as the vertex with the two sides of the crack as the edges, respectively. The discs with the diameter of 3 mm were cut 2 - 3 mm away from the fracture surface. They were ground to the thickness of about 50 μm by the abrasive paper. They were etched in a solution of 10% perchloric acid and 90% ethanol (volume percent) by a twin-jet electropolishing device at - 30 °C and 40 V. The dislocation structures were observed in a JEOL JEM-2010 transmission electron microscope (TEM) at an accelerating voltage of 200 kV.

3. Results

3.1. Creep-fatigue cyclic life and rupture time

Combined with our previous results (Ding et al., 2018b), long dwell times of 16, 32, 64, and 128 min at $\Delta\varepsilon_t$ of 1.6% and at 900 °C were further applied to verify the creep-fatigue N_f "saturation phenomenon" [Fig. 2(a)]. A pleasant surprise is that N_f no longer decreases, but even increases slightly with the increasing long dwell time. In this investigation, the factor of the strain range and the underlying mechanism influencing the occurrence of this crucial phenomenon were studied in detail. The relationship between the cyclic life (N_f) and dwell time with different $\Delta\varepsilon_t$ at 900 °C for the DZ445 superalloy are shown in Fig. 2(b). Compared with the cyclic life in the case of without dwell time, the cyclic life is all greatly reduced when 2, 3, 5, or 8 min dwell time are applied. While compared with the fatigue life at 2 min dwell time, as the dwell time reaches 5 and 8 min, N_f increases slightly (the values of $\Delta\varepsilon_t$ are 1.6% and 1.0%) or hardly further decreases (when the $\Delta\varepsilon_t$ is 0.6%). Thus, the generalized N_f "saturation phenomenon" is formed. In the creep-fatigue deformation of the GH4169 (Chen et al., 2016) and Incoloy-800H superalloy (Meurer et al., 1984), the phenomenon that cyclic life no longer decreases with increasing dwell time also appeared, but the relevant reason was not mentioned. In this study, this important phenomenon and its corresponding mechanism with different strain ranges are studied in detail.

For the cyclic life change in different strain ranges, the absolute and relative change amplitudes of N_f during different dwell periods (0 - 2, 0 - 3, and 0 - 8 min dwell time) are all listed in Table 2. When the values of $\Delta\varepsilon_t$ are 0.6%, 1.0%, and 1.6%, compared without dwell time, the absolute decrease amplitudes of N_f with a 2 - min dwell time are 15,384, 994, and 350; and the relative amplitudes for them are 0.7439, 0.5984, and 0.5882, respectively. Similarly, compared to those without dwell time, the relative decline amplitude of cyclic life for these strain ranges are 0.7648, 0.7285, and 0.6857 with 3 min dwell time and 0.7779, 0.6020, and 0.5781 with 8 min dwell time, respectively. The relative and absolute decline values of cyclic life with dwell time all decreases with the increasing strain ranges. Our results have shown that N_f saturation occurs when the dwell time reaches 8 min. For the time required to form the N_f saturation phenomenon under high strain range is shorter. This phenomenon was defined as that the N_f saturation phenomenon which is easier to occur. Therefore, the formation of N_f saturation is favored by the increase of $\Delta\varepsilon_t$. If the creep-fatigue data at different total strain ranges for the 316 L stainless steel (Novelo et al., 2008) and 9Cr-1Mo steel (Takahashi, 2008) are selected, it also conforms to the formation rule of the N_f saturation discussed above. However, the influence of strain ranges on the N_f saturation was not mentioned in previous studies.

The cyclic life is generally used to evaluate the creep-fatigue performance because it belongs to the category of low cycle fatigue.

Table 1
Creep-fatigue experiment parameters at different total strain ranges for the DZ445 superalloy.

Temperature (°C)	Strain range (%)	Dwell time (min)
900	0.6	0, 2, 3, 5, 8
900	1.0	0, 2, 3, 5, 8
900	1.6	0, 2, 3, 5, 8, 16, 32, 64, 128

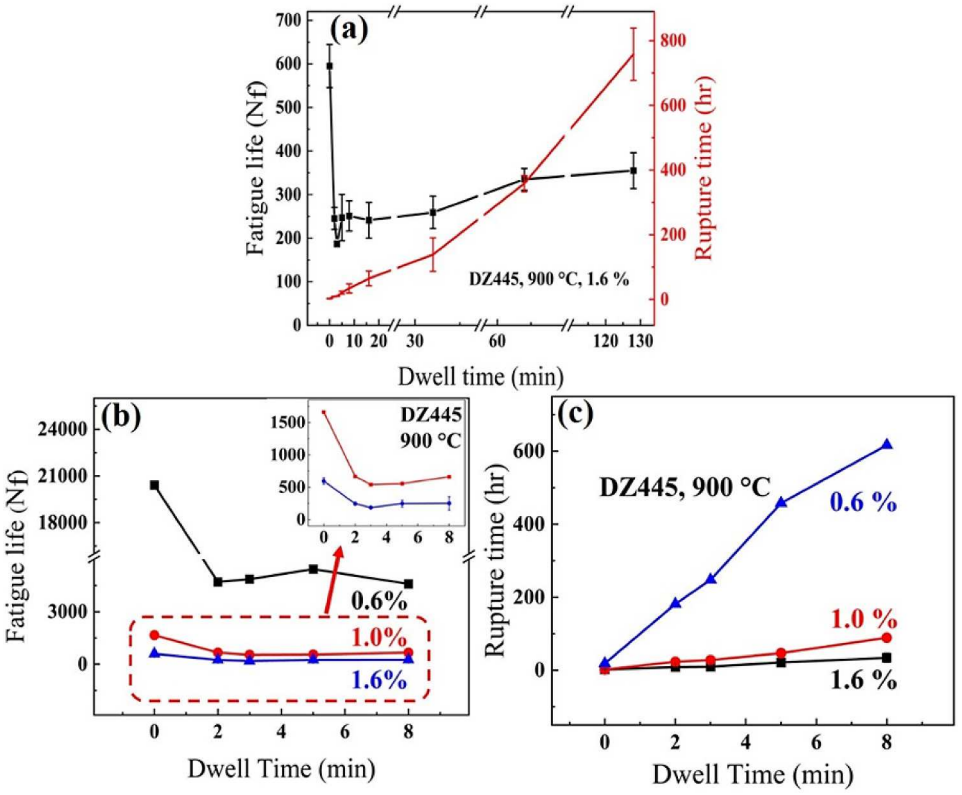

Fig. 2. Relationship between the dwell time and N_f (a and b) as well as t_f (c) with different conditions for the DZ445 superalloy. (The vignette in Fig. 2b is a magnification of the two higher conditions to properly observe the N_f saturation phenomenon. The N_f and t_f are defined as the number of cycles and the total experimental time until the sample is broken, respectively.).

Table 2
Change amplitude of cyclic life in different dwell-time periods with various conditions. The absolute change amplitude of the cyclic life, "A", is defined as $A = (N_{sub} - N_0)$. The relative change amplitude of the cyclic life, "R" is defined as $R = (N_{sub} - N_0)/N_0$, where N_{sub} is the cyclic life with long dwell time, and N_0 is the cyclic life without dwell time. The numbers in the lower right corner of "A" and "R" represent different dwell-time periods with the unit of minute.

Total train range /Variations of fatigue life	A_{0-2}	R_{0-2}	A_{0-3}	R_{0-3}	A_{0-8}	R_{0-8}
0.6%	15,384	0.7439	15,816	0.7648	16,088	0.7779
1.0%	994	0.5984	1210	0.7285	1000	0.6020
1.6%	350	0.5882	408	0.6857	344	0.5782

This research shows that N_f gradually saturates with the increase of the dwell time [Figs. 2(a and b)], which implies the limitation of the case that N_f is the only indicator when the N_f saturates with long dwell time. The rupture time is an important durability concern for service. In the creep-fatigue deformation, the rupture time shows the relationship with cyclic- life (Nagae, 2013),

$$t_f = N_f \times \left(\frac{2\Delta\varepsilon}{\dot{\varepsilon}} + t_d\right) \tag{1}$$

where t_d, $\Delta\varepsilon_t$, and $\dot{\varepsilon}$ are dwell time, total strain range, and strain rate during the loading/unloading stage, respectively. It is worth noting that t_f increases continually with dwell time [Fig. 2(a)]. The same phenomenon of t_f with dwell time for different strain ranges are also shown in this investigation [Fig. 2(c)]. It is because the N_f is saturated with the long dwell time, and the factor of the dwell time in Eq. (1) is much longer than that of the loading/unloading time in a single cycle. Therefore, when the cyclic life is saturated with long dwell time, the rupture time could be used as a supplementary index to evaluate the creep-fatigue performance well.

3.2. Mechanical response

3.2.1. Maximum tensile-stress response

After achieving the interesting and important phenomenon in the creep-fatigue deformation with different strain ranges, it

naturally follows to analyze the mechanisms lying behind the N_f "saturation phenomenon". The mechanical response involving the maximum tensile stress, mean stress, hysteresis loop, stress-relaxation process, and damage features, such as fracture surface, longitudinal cracks, internal voids, evolution of γ' precipitate, and dislocation structures will be analyzed in detail below.

The interaction between dislocations-dislocations and dislocations-precipitates is reflected in the dynamic competition of cyclic softening/hardening (He et al., 2017). The function of the maximum tensile stress vs. cyclic number with different strain ranges are shown in Fig. 3. Regardless of what $\Delta\varepsilon_t$, the maximum tensile stress is the highest, and N_f is the longest without the dwell time. With the application of the dwell time, the maximum tensile stress decreases rapidly, and the N_f is also greatly reduced. Maximum tensile stresses with dwell times of 5 and 8 min are close to each other in the same strain range. There is also no big difference in the fatigue life of this condition. Thus, it results in the appearance of the "saturation phenomenon" for cycle life. The fluctuation of maximum tensile stress may be related to the appearance of micro-cracks, which will be given in detail in Section 3.3.

In order to show the influence of the total strain ranges on the N_f "saturation phenomenon" clearly, the maximum stress responses for 0 - 8 min dwell time under different $\Delta\varepsilon_t$ are shown in Fig. 3. The characteristic cycle in Fig. 3 is defined as the turning point between the initial rapid softening and the subsequent slight softening/hardening of the maximum tensile stress, which represents the transition from the unstable state (the rapid generation of dislocations) to the steady state (the dynamic equilibrium of the generation and annihilation of dislocations) during deformation (Ding et al., 2021). When the values of $\Delta\varepsilon_t$ are 0.6%, 1.0%, and 1.6% [Figs. 3(a), (b), and (c)], the maximum tensile stresses without dwell time at characteristic cycles are 291 MPa, 367 MPa, and 595 MPa, respectively. Those values are 146 MPa, 241 MPa, and 331 MPa with 8-minute dwell time, respectively.

In the creep-fatigue deformation, the fatigue-crack-growth rate can be described by the amplitude of the stress intensity factor (ΔK_1) (Zhang et al., 2007). The stress intensity factor is proportional to the stress amplitude ($\Delta\sigma$), as given in Eq. (2),

$$\Delta K_1 \propto \Delta\sigma \tag{2}$$

where a higher stress amplitude results in a faster rate of crack propagation, and then lower fatigue life. Thus, less time are required to reach N_f saturation at high strain-ranges. That is, the N_f "saturation phenomenon" is faster to occur.

The variation amplitude of the maximum tensile stress (SVA) with 8-minutes dwell time is defined as follow,

$$SVA = (\sigma_0 - \sigma_8)/\sigma_0 \tag{3}$$

where σ_0 and σ_8 are the maximum tensile stress at the characteristic cycle with the dwell times of 0 and 8 min, respectively. Thus, the corresponding relative reduction amplitudes for them are 0.4983, 0.3433, and 0.4437, respectively. These changes in SVA indicates that the impact of σ_{max} on cyclic life with dwell time is the most drastic in the case of 0.6%. That is, the cyclic life decreases the most.

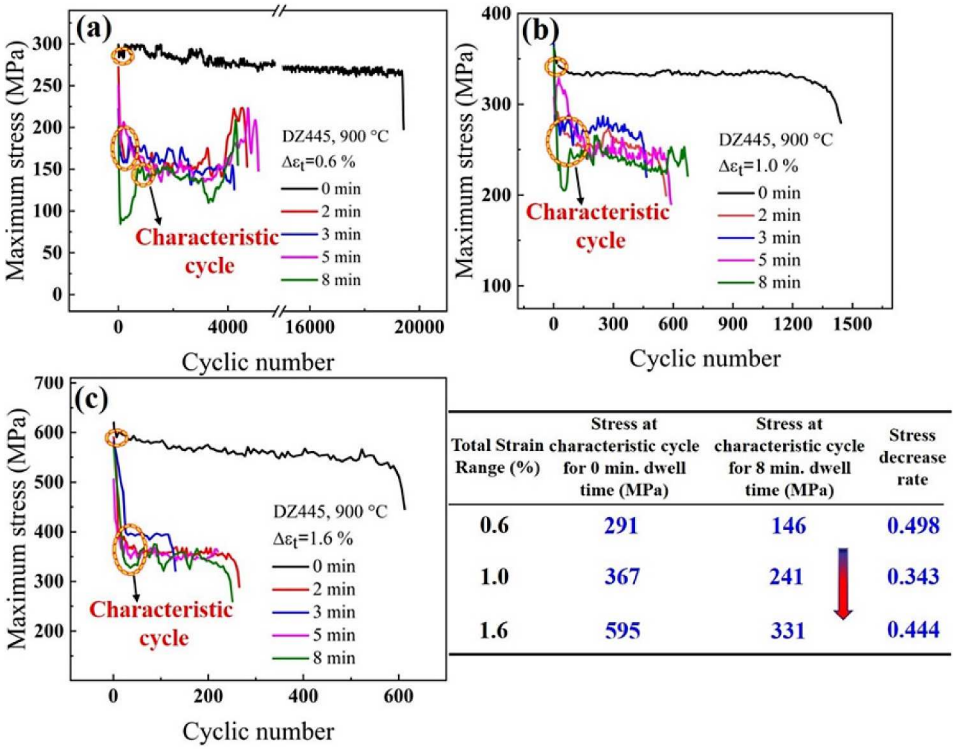

Total Strain Range (%)	Stress at characteristic cycle for 0 min. dwell time (MPa)	Stress at characteristic cycle for 8 min. dwell time (MPa)	Stress decrease rate
0.6	291	146	0.498
1.0	367	241	0.343
1.6	595	331	0.444

Fig. 3. Relationship between the maximum tensile stress and cyclic number for DZ445 superalloy at characteristic cycles under different total strain ranges.

The relative reduction amplitudes of σ_{max} between 0 - 2 and 0 - 3 min dwell periods with other strain ranges in Table 3 also shows the same trend. However, it seems that in the strain range of 1.0% and 1.6%, the relative change of maximum stress with dwell time is somewhat contrary to the change trend of cyclic life. In addition to the evolution of the maximum tensile stress per cycle, it is well known that creep - fatigue life is also closely correlated with the mean stress.

3.2.2. Mean stress

The mean stress, σ_m, was calculated as the average level of the maximum and minimum stress [i.e. $\sigma_m = (\sigma_{max} + \sigma_{min})/]$. In fatigue deformation, some studies cover mean stress correction methods for various fracture modes and factors such as stress ratio, material, and environment (Zhu et al., 2017). In creep-fatigue deformation, compressive mean stress occurred when a tensile-dwell time was applied, indicating that the peak compressive stress was greater than the peak tensile stress. This compressive mean stress was present due to the stress relaxation during the tensile dwell-period of each cycle. Thus, a higher compressive stress to close the hysteresis loop are required due to the reversal of relaxation-induced inelastic strains (Lord et al., 1973). The mean stress magnitude is affected by different factors, such as the ratio of elastic to inelastic strain and dwell time, etc. (Zhang et al., 2014). Fig. 4 shows the mean stress vs. cyclic number with different dwell times at various strain ranges during creep-fatigue deformation. It can be seen that no matter what strain ranges, the mean stress was close to zero for the case without a dwell time, while the compressive mean stresses occurred when a dwell time was applied. Ostergren (Ostergren et al., 1976) and Brinkman (Brinkman et al., 1976) concluded that negative compressive mean stress has a healing effect on tensile tests of different materials by comparing with the positive mean stress in the compressive strain-only dwell test. In order to explain this phenomenon, Prof. Tu and Zhang (R.Z. Wang et al., 2016 and 2017) assumed that in the energy model, only the tensile part above the absolute value of the mean stress in the dwell stage will produce creep damage ($\sigma > -\sigma_m$). The inelastic strain energy density ($W_{in,new}$) in dwell stage under a certain cycle representing creep damage can be written as: $W_{in,new} = \frac{\sigma_0^2 + 2\sigma_m \cdot \sigma_0 - 2\sigma_m \cdot \sigma - \sigma^2}{2E}$, where σ_0, σ, σ_m, and E are the initial stress and the ending stress in the dwell period, the mean stress, and the elastic modulus, respectively. It can be seen from this equation that under a certain cycle in the creep-fatigue deformation process, when the initial value of stress relaxation and the amount of stress relaxation in the dwell stage are constant, the greater absolute value of the compressive mean stress, σ_m, results in the smaller the energy consumed by creep damage in one cycle. It leads to the longer cycle life. Combined with the results of our creep-fatigue test on DZ445 superalloy in this study, the absolute value of the compressive mean stress under the dwell time of 8 min is the largest in Fig. 4(b) and (c). The variation trend of the maximum tensile stress (σ_{max}) with the cycle life in Fig. 3 shows that the σ_{max} under the 8-minute dwell time is also lower than the σ_{max} value with the short dwell time. The stress relaxation results of Fig. 6 in the subsequent section also show that the stress relaxation values at 1.0% and 1.6% total strain ranges are saturated for both 8 min and short dwell times. Therefore, according to the above model proposed by Tu and Zhang, the energy dissipation of the DZ445 superalloy responsible for creep damage under the 8-minute dwell time is lower than the value under the short dwell time, so the saturation phenomenon of cyclic-life appears. However, under the condition of 0.6% total strain range as shown in Fig. 4(a), the mean stress in the 8-minute dwell period is similar to that under short dwell time (such as 2 and 3 min). And as shown in Fig. 6, the amount of stress relaxation under 8 min dwell condition is greater than the value under the short dwell time. Therefore, in the 8-minute dwell time condition, more energy is consumed per cycle. The corresponding cyclic-life continues to decrease. That is, the creep-fatigue cycle life at 0.6% total strain range is difficult to reach saturation. Meanwhile, it can be seen from Fig. 4(b) and (c) in this investigation that the mean stress becomes stable rapidly. However, the stress in Fig. 4(a) fluctuates greatly with the cyclic number. It means that the evolution of mean stress with the number of cycles shows that the creep-fatigue life is more likely to saturate with long dwell time at high strain ranges (1.0% and 1.6%) conditions than that in the condition of 0.6% total strain range.

However, the above explanation about the mean stress seems to contradict the phenomenon that the longer the dwell time is, the larger the creep damage is under the constant strain-dwell period. In response to this problem, our previous research results show that both tensile and compressive stress can contribute to creep-fatigue damage (Ding et al., 2019). It is not just the stress in the tension part contributes to the damage. Under certain loading conditions, the proportion of these two contributions to the damage can be given quantitatively. Thus, our interpretation of mean stress here is reasonable. As a criterion of creep-fatigue life, the stress response does not seem to be the most accurate. The hysteresis loop is a comprehensive manifestation of stress and strain parameters, the area of which is usually used as a measure of the inelastic strain energy (Chen et al., 2016).

3.2.3. Hysteresis loop

As shown in Fig. 5, the area of the hysteresis loop in the characteristic cycle with dwell time is much larger than that under pure-fatigue deformation regardless of what total strain ranges. A similar area with dwell time corresponds to the semblable consumed energy during deformation, indicating that N_f is saturated. The inelastic strain energy is expressed as,

Table 3
Statistics of maximum tensile stress response at characteristic cycles during different dwell time periods for DZ445 superalloy under different total strain ranges.

Total strain range (%)/σ_{max} (MPa)	σ_{max} for 0 min.	σ_{max} for 2 min.	σ_{max} for 3 min.	σ_{max} for 8 min.	σ_{max} decrease rate for 0–2 min	σ_{max} decrease rate for 0–3 min	σ_{max} decrease rate for 0–8 min
0.6	291	171	161	146	0.4124	0.4467	0.4983
1.0	367	269	264	241	0.2670	0.2807	0.3433
1.6	595	375	400	331	0.3694	0.3277	0.4437

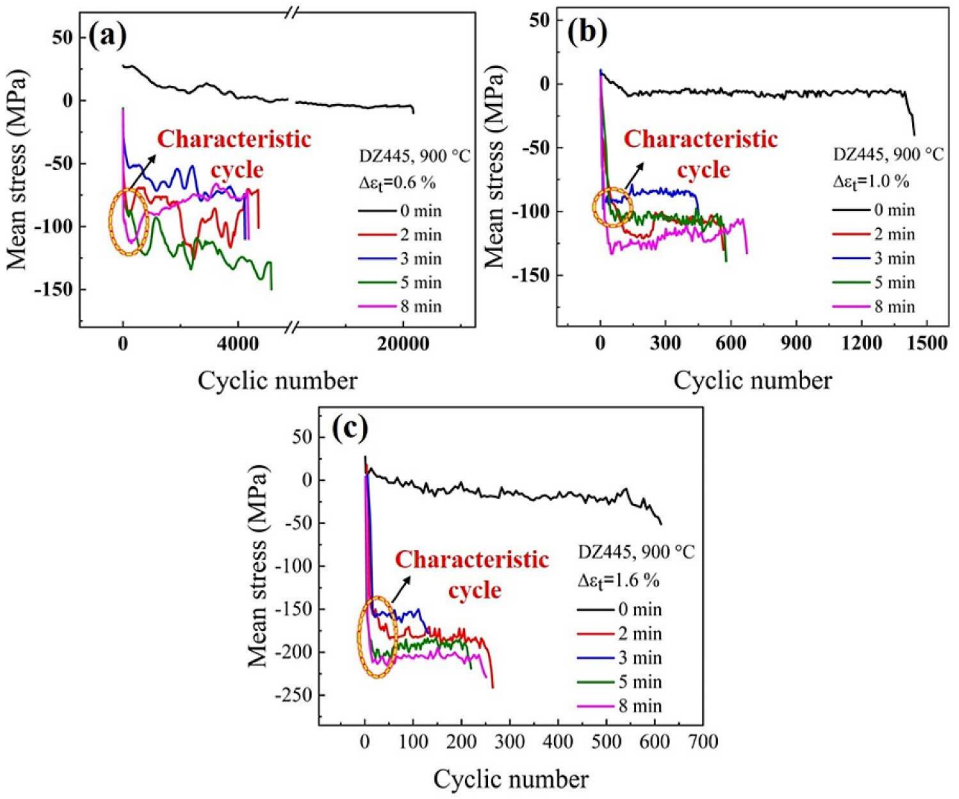

Fig. 4. Mean stress as a function of cyclic number for directionally solidified Ni-based superalloy DZ445 samples with different dwell times at various strain ranges.

$$\Delta U_{in} = \alpha \times \sigma_T \times \Delta\varepsilon_{in} \tag{4}$$

where α, σ_T, and $\Delta\varepsilon_{in}$ are shape factor, maximum tensile stress, and inelastic strain, respectively. The values of σ_T and $\Delta\varepsilon_{in}$ under different conditions can be obtained from the mechanical response in Figs. 3 and 5. Halford proposed the expression of the shape coefficient as (Halford, 1966),

$$\alpha = 1/1 + n' \tag{5}$$

where n' is the cyclic strain-hardening index, which is determined by the cyclic stress-strain curve obtained from the pure low-cycle-fatigue experiments. The variation amplitude of the corresponding the inelastic strain energy with 8 min dwell time is defined as follows,

$$HIA = |(S_0 - S_8)/S_0| \tag{6}$$

where S_0 and S_8 denote the inelastic strain energy with dwell times of 0 and 8 min, respectively. As shown in Fig. 5(d), when the total strain ranges are 0.6%, 1.0%, or 1.6% (the corresponding S_0 are 0.04625 MJ/m^3, 0.2911 MJ/m^3, or 0.7705 MJ/m^3, and the corresponding S_8 are 0.1214 MJ/m^3, 0.5573 MJ/m^3, or 1.150 MJ/m^3, respectively), the relative increase amplitudes are 1.62, 0.91, or 0.49, respectively. Thus, with the increase of $\Delta\varepsilon_t$, the impact of inelastic strain energy on the cyclic life with the dwell time is reduced when a 8-minutes dwell time is applied. Small changes in consumed energy results in the easier creation of the N_f "saturation phenomenon" at a larger strain range.

The Holloman equation is usually used to relate the cyclic stress and the plastic strain in hysteresis loop (McDaniels et al., 2011),

$$\sigma_a = K_2' (\varepsilon_p)^{n_2'} \tag{7}$$

where σ_a, K_2', ε_p, and n_2' are the stress amplitude (MPa), material constant (MPa), plastic-strain amplitude, and strain-hardening exponent (positive number). Thus, the high strain-range results in large plastic strain range and stress amplitude, followed by the shorter fatigue life. It takes less time to reach N_f saturation. That is, the N_f "saturation phenomenon" occurs more easily with the increasing strain ranges. The change of the hysteresis loop area (inelastic tensile strain energy) is attributed to the stress-relaxation process during the tensile-dwell period. Therefore, the influence of the stress-relaxation behavior on the N_f "saturation

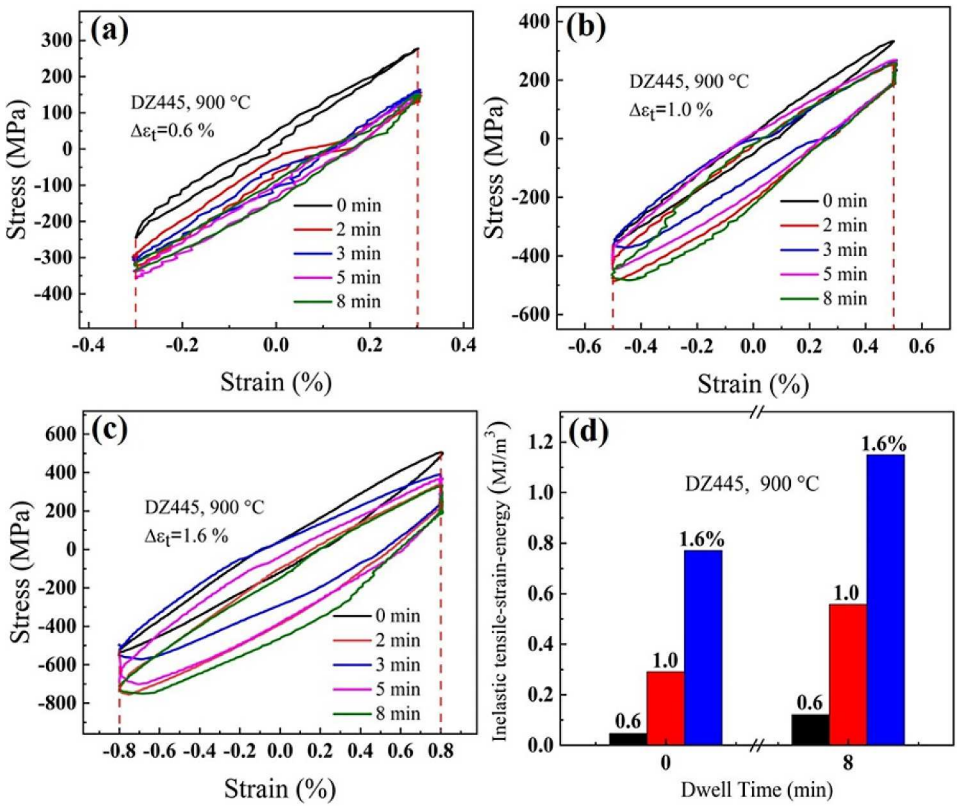

Fig. 5. Comparison of the hysteresis loop and corresponding area (inelastic tensile strain energy) of DZ445 superalloy at characteristic cycles under different strain ranges.

phenomenon" will be further analyzed in the following sections.

3.2.4. Stress-relaxation process during the dwell period

In the creep-fatigue test, some scholars believed that the whole dwell periods result in the additional creep damage (Fan et al., 2015a). Others believed that fatigue damage was caused by the initial rapid stress-relaxation, and only the steady stage of relaxation will cause creep damage (Rodriguez and Rao, 1993). Fig. 6 shows the stress vs. dwell time curve for the DZ445 superalloy subjected to different tensile-dwell periods at the characteristic cycles with different total strain ranges. These stress-relaxation curves show three stages: the initial rapid softening, the subsequent transition, and the final stability.

In order to show the phenomenon of total strain ranges on stress relaxation more clearly, the statistical results of initial value, ending value, and stress-relaxation amount during stress-relaxation period under different conditions are shown in Fig. 6. In order to unify the comparison criteria, the stress relaxation values at 8-minute dwell time are chosen as a reference. Since the amount of stress relaxation is also related to the initial value of relaxation, the ratio of relaxed stress to the initial value of relaxation are also compared. The results show that the amount of stress relaxation increases with the increase of strain range. At 900 °C and with $\Delta\varepsilon_t$ of 0.6%, 1.0%, and 1.6%, the relaxed stresses are 130 MPa, 189 MPa, and 211 MPa with 8-minutes dwell time. Their proportions to the corresponding stress-relaxation initial value are 0.1096, 0.2158, and 0.3567, respectively [Figs. 6(d)]. These two parameters are both increased with increasing $\Delta\varepsilon_t$, indicating that more damages are caused. Under high strain ranges, the greater creep-fatigue damage results in the shorter time to reach N_f saturation. Therefore, the N_f "saturation phenomenon" appears more easily at high strain ranges. The change of stress response is essentially caused by the evolution of microstructure and dislocation. The effect of strain range on damage mechanism will be analyzed as follow.

3.3. Fractography

The fracture feature of creep-fatigue interactions contains both characteristics of low-cycle fatigue and pure creep fracture. Previous literature reported that the fracture of the pure low-cycle fatigue in superalloys originates from the surface, and the crack-propagation area is relatively flat (Shi et al., 2013). Creep-deformation cracks originate from inside the sample, such as topologically close-packed (TCP) precipitates or cracked carbides, etc. (Reed. et al., 2007). When the fatigue cracks meet the creep voids, the aggregation and growth rate of the fatigue cracks would be accelerated in creep-fatigue deformation.

The partial and full view of fracture with different strain ranges at 900 °C are shown in Fig. 7. There is an obvious crack-initiation

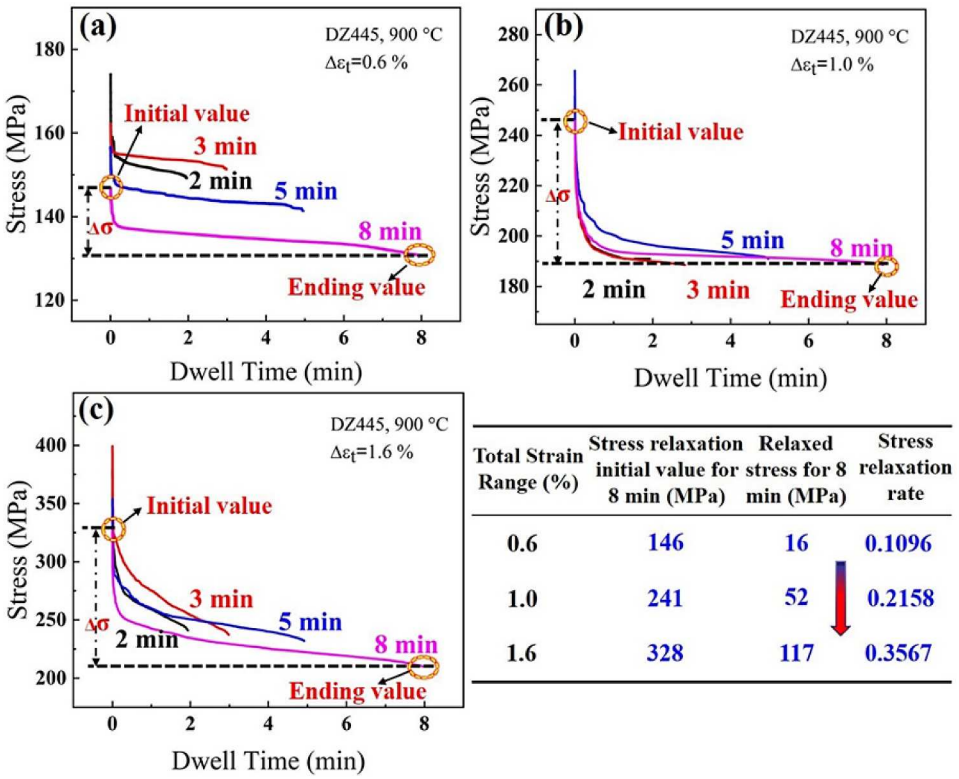

Total Strain Range (%)	Stress relaxation initial value for 8 min (MPa)	Relaxed stress for 8 min (MPa)	Stress relaxation rate
0.6	146	16	0.1096
1.0	241	52	0.2158
1.6	328	117	0.3567

Fig. 6. Stress-relaxation curves of the DZ445 superalloy under different conditions during the dwell period at characteristic cycles. (Due to the large fluctuation of stress-relaxation curves in the figure, we fitted the data properly. The amount of stress relaxation is the difference between the initial and the final value during a dwell period.).

area and typical fatigue stripes on the fracture surface without dwell time [Figs. 7(a) and (b)]. The crack-propagation region is relatively flat and the transient-fracture region is opposite to the crack-initiation region. It is consistent with the typical feature of the pure-fatigue fracture (Miao et al., 2009). The cyclic life is long in the case of pure fatigue. As the dwell time increases to 3 min [Figs. 7 (c) and (d)], there are some cavities with creep characteristics and cleavage-like facets as well as fatigue striations. Their interactions between fatigue cracks and creep voids promote each other, reducing the cyclic life. Gordon (Gordon et al., 2006) also found that for GTD-111 superalloy, the dwell period can promote the interconnections between the cavities. In the case of 8-min dwell time, the fatigue stripes disappear. The proportion of plastic deformation characteristics increases greatly. A large number of intergranular cracks, dimples, and tearing edges are present [Figs. 7(e) and (f)]. These dimples delay the propagation of cracks. Thus, the cyclic life will not be further reduced. That is, no matter what strain ranges, the saturation phenomenon of cyclic life will appear with long dwell time.

As the total strain range increases from 0.6% to 1.0%, whether it is 0, 3, or 8 min dwell time, as shown by the yellow dotted line in the illustration at the upper right corner of Fig. 7, the area of crack-initiation and -propagation region decreases with the increase of strain range at the same dwell time. The fatigue life of cyclic deformation is mainly consumed in the crack initiation and propagation stage (Fleury et al., 1994). Therefore, the fracture feature also corresponds to the decrease in cyclic life with the increase of strain range well. That is, the time required to reach N_f saturation at high strain is shorter. The saturation phenomenon of cyclic life is easier to appear with the increase of strain range.

In order to further investigate the influence of strain ranges on the crack-propagation path, the SEM images of the fracture profile are shown in Figs. 8 and 10. In the creep-fatigue deformation, the slender surface cracks perpendicular to the stress are mainly generated without the dwell time [Figs. 8(a-a´´)]. The typical fatigue and creep cracks are characterized by originating from the sample surface (León-Cázares et al., 2020b) or inside (Darling et al., 2016), respectively. With the dwell time increased to 3 min [Figs. 8 (b-b´´)], the cracks gradually become blunted. There are also some tiny cavities. In the case of 8 min dwell time [Figs. 8(c-c´´)], the blunted crack and micro-voids is greatly increased. These characteristics show that the application of dwell time promotes the cyclic softening of material, leading to an increase in plastic zone.

Both the length and opening angle of cracks are the manifestations of damage (Miao et al., 2009). The distribution characteristics of cracks within 1 mm below the fracture were statistically analyzed and shown in Fig. 9. Compared with the case without dwell time, the cracks with length more than 100 μm and opening angle more than 15 ° is greatly increased with 8 min dwell time. Thus, the increased creep-fatigue damage decreases the cyclic life. In the low strain range, the damage with short cracks is dominant regardless of what dwell time. The damage distribution is more uniform and the cyclic life is longer. However, in the case of high strain range, long cracks

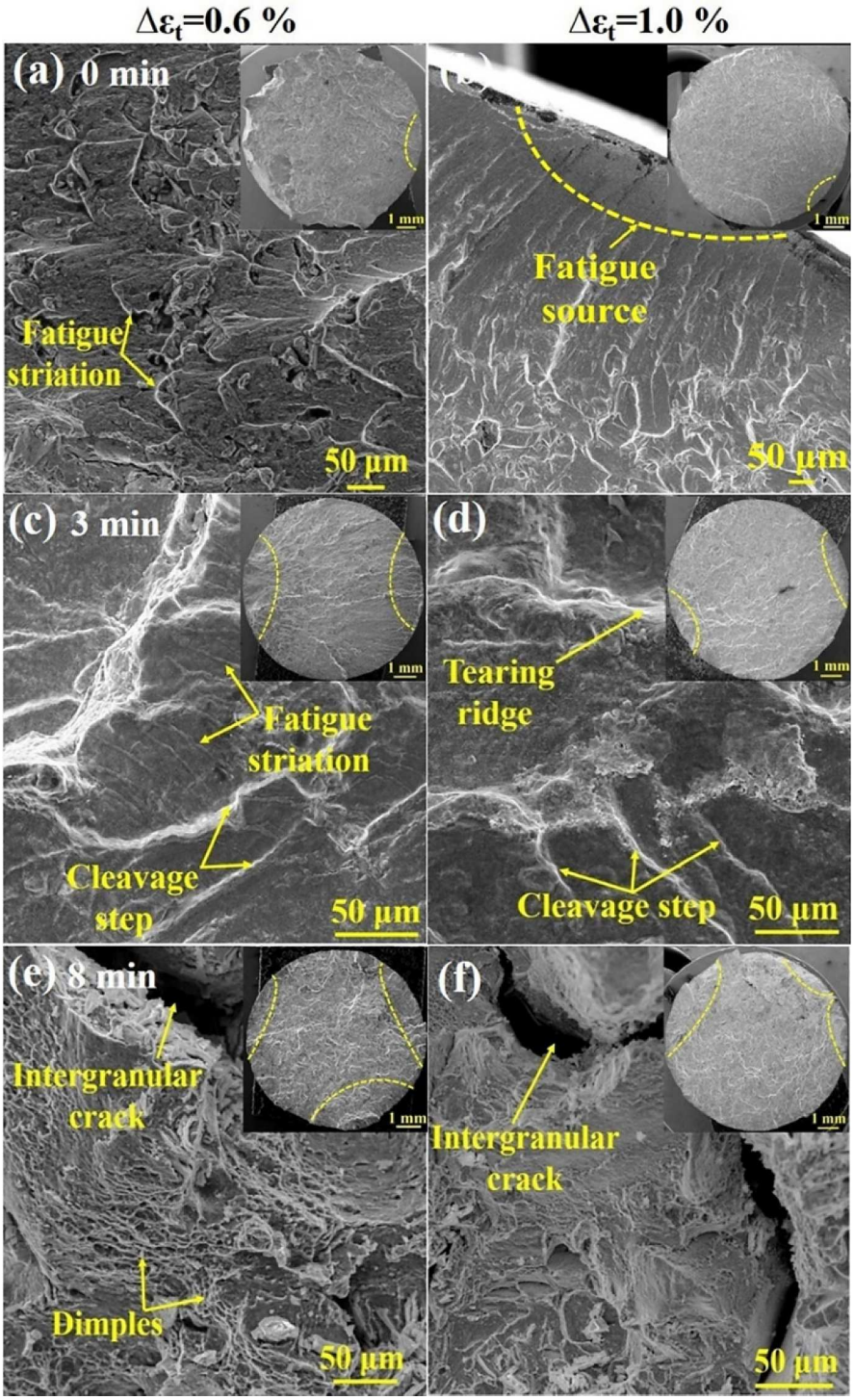

Fig. 7. Partially-enlarged views of the creep-fatigue fracture for the DZ445 superalloy with different total strain ranges at 900 °C. (The illustration in the upper right corner of the figure is the overview of fracture. The area indicated by the yellow dashed line is the crack-initiation area).

are dominant, and their number is less than that of low strain-range. The damage is mainly localized and the corresponding cyclic life is short. Correspondingly, it takes less time to reach N_f saturation, which results in the easier formation of the N_f "saturation phenomenon" with high strain ranges.

The creep-fatigue crack-growth rate can be decomposed into two components as the cycle-dependent crack-growth rate, $\left(\frac{da}{dN}\right)_f$, and

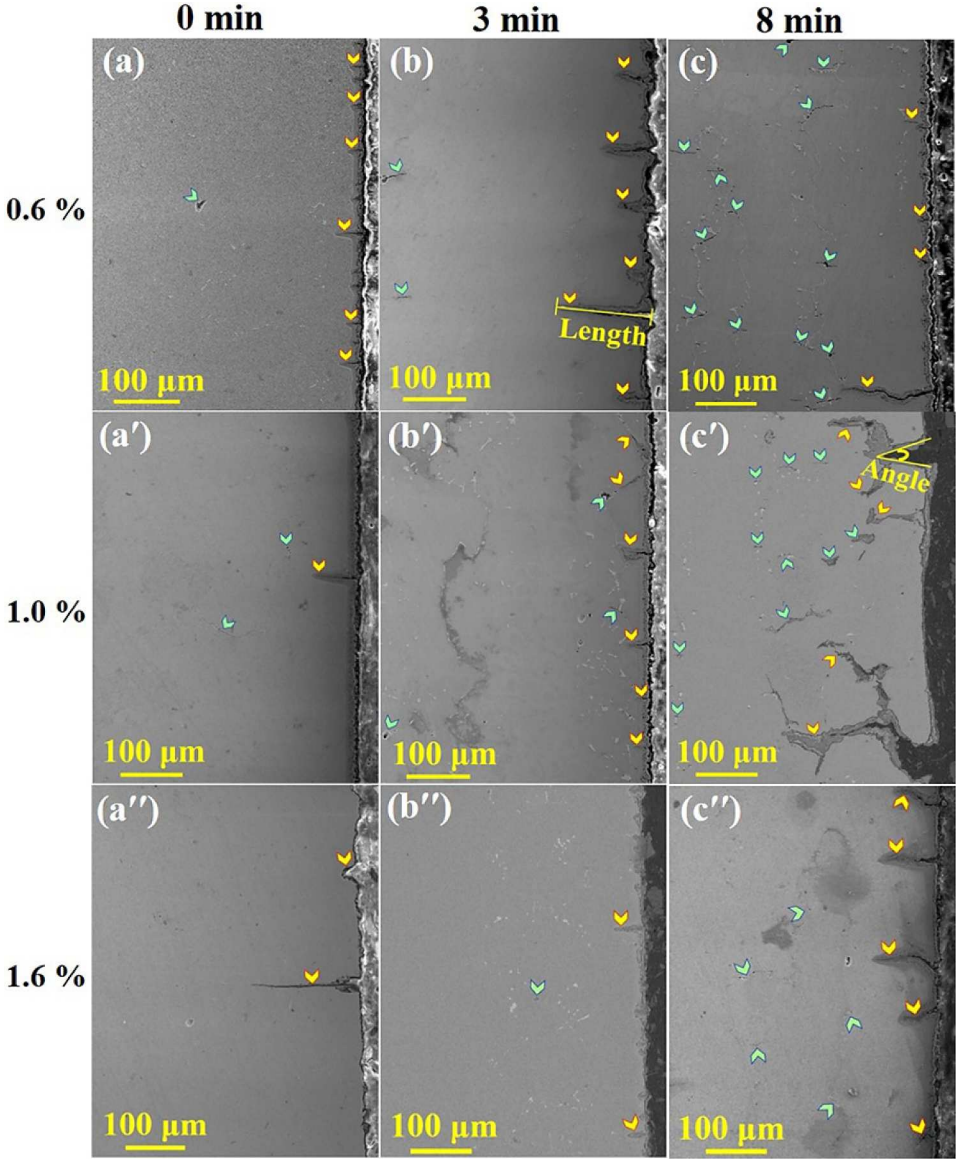

Fig. 8. Longitudinal cracks and internal voids of the creep-fatigue fracture for the DZ445 superalloy under different total strain ranges at 900 °C. (The yellow and green arrows indicate the lateral cracks and internal voids, respectively.).

the time-dependent crack-growth rate, $\left(\frac{da}{dN}\right)_t$. From the fracture observation of Figs. 8(a-a′′), only a small part of creep deformation could be found at the crack tip of high-temperature low-cycle fatigue. Thus, the fatigue crack-growth rate can be expressed by the amplitude of the stress intensity factor (ΔK), i.e.,

$$\left(\frac{da}{dN}\right)_f = C_3(\Delta K_3)^{m_3} \tag{9}$$

Then, the total crack-growth rate is,

$$\left(\frac{da}{dN}\right) = C_3(\Delta K_3)^{m_3} + \left(\frac{da}{dN}\right)_t \tag{10}$$

where C_3 and m_3 are constants, which are related to the material, wave form, and environment. It can be seen from Eqs. (9) and (10) that under the same dwell time, the greater stress amplitude results in the greater stress intensity factor. Thus, the greater the fatigue-crack-growth rate is obtained. Therefore, the cycle life is reduced with the increase of the total strain range.

In addition to the lateral cracks, the internal voids are also the important manifestations of creep-fatigue damage. Brinkman

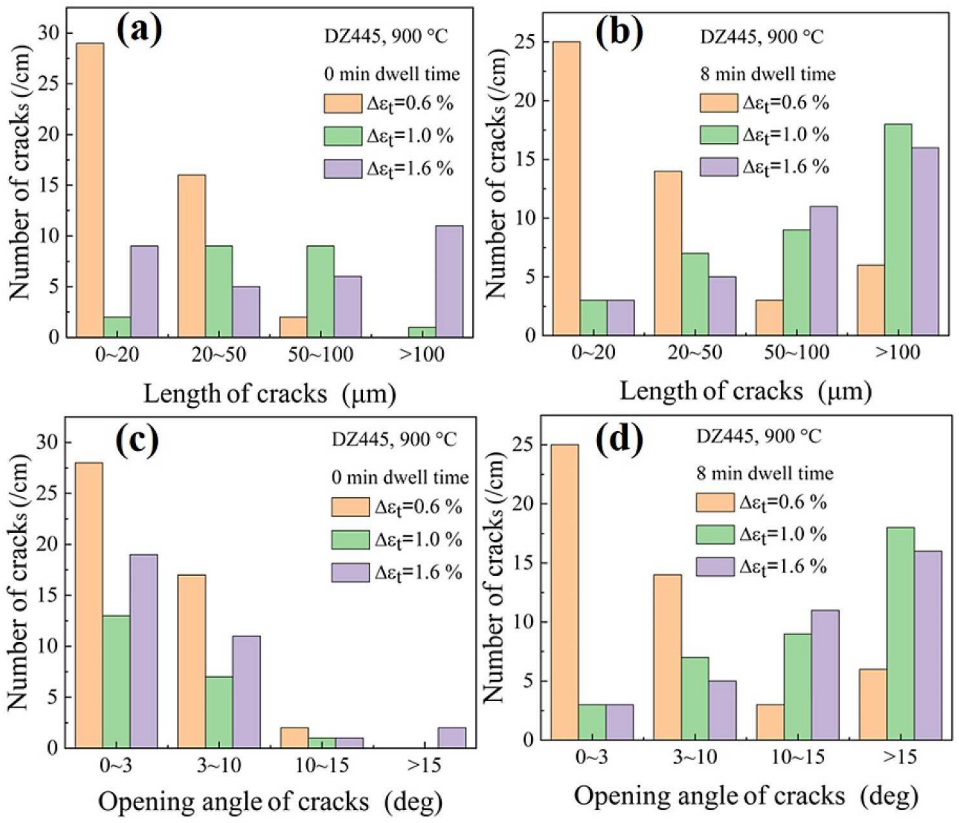

Fig. 9. The distribution characteristic statistics of longitudinal cracks in the creep-fatigue fracture for DZ445 superalloy under different total strain ranges at 900 °C.

believed that the N_f "saturation phenomenon" is caused by the delay of the void interconnection (Brinkman and Korth, 1973). The occurrence of lateral cracks is closely related to cyclic loading (Joseph et al., 2020), while the application of the dwell time would cause more internal damage associated with the time-cumulative effect (Tang et al., 2017a). In order to reflect the influence of strain range and dwell time on internal damage more specifically, the representative images and corresponding statistical results of the area distribution for the internal voids are shown in Figs. 10 and 11. At 900 °C and with the total strain ranges of 0.6%−1.6%, few internal voids are appeared in low-cycle-fatigue deformation because there is not sufficient time for the voids to nucleate and grow [Figs. 10 (a-a´´)]. With 3 min of dwell time [Figs. 10(b-b´´)], few voids distributed along the grain boundaries are caused by the increased test time. As dwell time increases to 8 min [Figs. 10(c-c´´)], the size of internal voids gradually becomes larger, which corresponds to increased experiment-time shown in Fig. 2(a).

The area-size distribution in Fig. 11 also shows that the internal damage in the form of creep voids introduced during 8 min dwell period not only provides additional crack-initiation sites but also the bridging connections to accelerate crack propagation under the tensile stress. The growth of wedge cracks and the development of voids require the plastic strain introduced during dwell periods. These mixture characteristics of the ductile- and creep- failures explain the N_f "saturation phenomenon" well.

At the same time, compared with the internal cavities under high strain range, the number of internal cavities with different sizes at low strain range is increased and the distribution is more uniform. At the high strain range of 1.6%, there is not enough deformation time to form more internal cavity damage. The localized-damage distribution is more obvious. At the low strain level (0.6%), the maximum stress response is low. Before the fracture of the main crack, the growth of voids is related to the time-dependent creep deformation. There is enough time for the voids and secondary cracks to grow after the nucleation, which corresponds to the large size of internal voids and cracks. When the strain level is high (1.6%), the internal voids do not have enough time for the nucleation, growth, and interconnection to the internal cracks. The size of internal voids is also small when the main crack is fractured. These localized damages indicate that the N_f "saturation phenomenon" occurs more easily with increasing $\Delta\varepsilon_t$, as shown in Fig. 2(b).

3.4. *Evolution of the γ' phase*

The existence of strengthening phase γ is the key factor to maintain the excellent properties of superalloy at high temperature (Van Sluytman and Pollock, 2012). The combined effect of stress and temperature will change the morphology of the γ′ phases. The morphology of the γ' precipitate for DZ445 superalloy after creep-fatigue deformation with different strain ranges is presented in

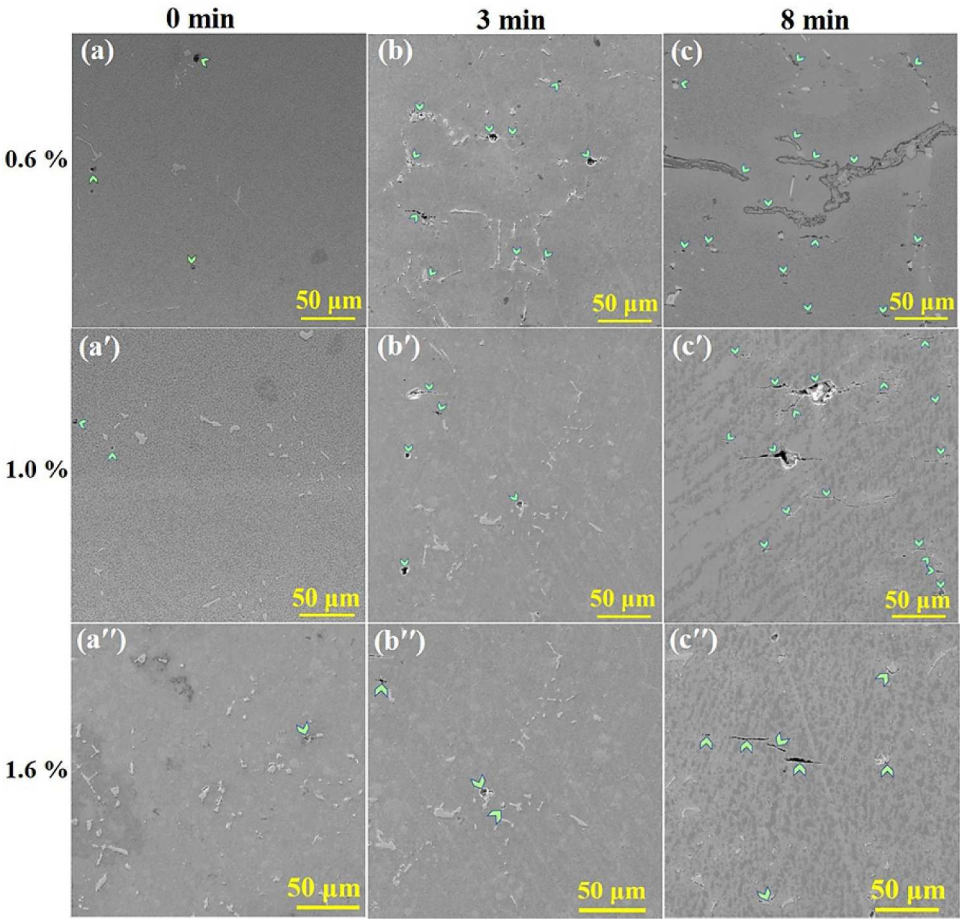

Fig. 10. Internal cavities of the creep-fatigue fracture for the DZ445 superalloy under different total strain ranges at 900 °C. (The green arrows indicate the internal voids.).

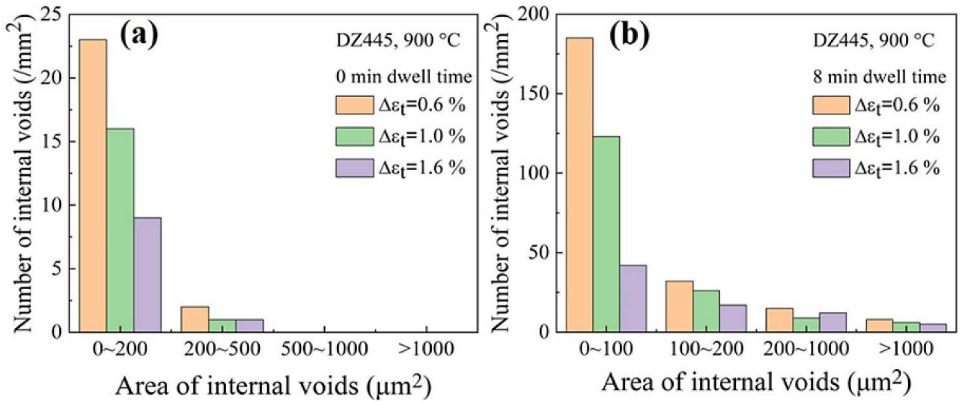

Fig. 11. The distribution characteristic statistics of longitudinal cracks in the creep-fatigue fracture for DZ445 superalloy under different total strain ranges at 900 °C.

Fig. 12. A small amount of γ' phases keeps the original cubic morphology, and most γ' phases are coarsened without dwell time [Figs. 12(a) and (b)]. After applying a dwell time of 3 min, γ' becomes rafted gradually. But it is more prone to raft at the total strain range of 0.6% than that of 1.0%, which is related to the longer deformation time at 900 °C [Figs. 12(c) and (d)]. When the dwell time reaches 8 min, the rafting becomes more complete due to more test time at high temperatures [Figs. 12(e) and (f)]. The rafting is the result of the simultaneous appearance of Ostwald-ripening-kinetics and directed-coalescence (Kirka et al., 2015). The partial loss of a

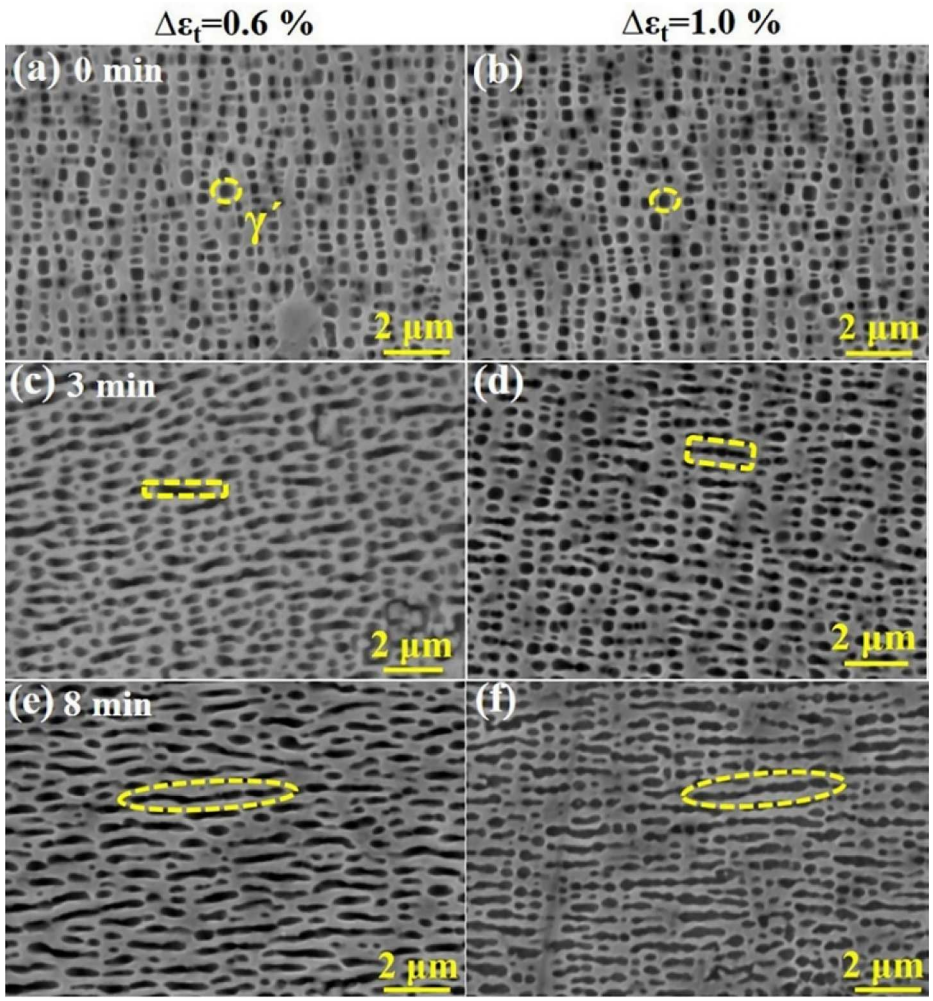

Fig. 12. The morphology evolution of γ' precipitates for the DZ445 superalloy with different total strain ranges at 900 °C after creep-fatigue deformation. (The yellow dotted lines indicate the γ' precipitate.).

coherence relationship between the γ/γ' interface caused by γ' coarsening makes it easier for the dislocations to shear the γ' phase. Although both rafting and coarsening are considered to be detrimental to the creep-fatigue properties of superalloys (Fan et al., 2015b). However, in the case of long dwell time, the cyclic life will not be reduced because the dislocation networks could hinder the movement of the subsequent dislocation, which will be explained in detail below.

The development of cracks, internal voids, and precipitates are the factors influencing the behavior of creep-fatigue (Conway et al., 1973 and Wareing, 1981). However, more researchers believe that the creep-fatigue behaviors are more close to the dislocation characteristic (Stinville et al., 2018). Then, the behind mechanism of the dislocation movement for the creep-fatigue N_f "saturation phenomenon" will be systematically discussed.

3.5. Dislocation structures

The differences in the mechanical responses and damage mechanisms are essentially caused by the dislocation movement. The plastic deformation during the low-cycle fatigue process is mainly produced by dislocation slipping and climbing. At 900 °C and with a $\Delta\varepsilon_t$ of 0.6%, dislocations are first generated in the γ matrix without the dwell time [Fig. 13(a)]. Due to the low applied stress of about ± 280 MPa (Fig. 3), the critical shear stress cannot be reached when the dislocations encounter the γ′ phase. The dislocations bypass γ′ mainly in the form of a climb. These uniform deformation characteristics result in long N_f. With a 3-min dwell time [Fig. 13(c)], some superdislocations cut into γ′ phase in the form of the antiphase boundary (APB) when the critical shear stress of γ′ is reached. The yellow arrows indicate the straight single superdislocations cutting into the γ′ phase. The blue arrows indicate the curved edge dislocations that isn't easy to slip on the (001) plane in the γ′ phase. Since these locked dislocations are relatively few, it is approximated that only the mobile straight superdislocations contribute to the inelastic strain rate ($\dot{\varepsilon}_{in}$) in the creep-fatigue deformation (Hirth and JohnPrice, 1983). Therefore, the $\dot{\varepsilon}_{in}$ is proportional to the density for the mobile straight superdislocation ($\dot{\varepsilon}_{in} = \rho_m bv$) (Tang et al.,

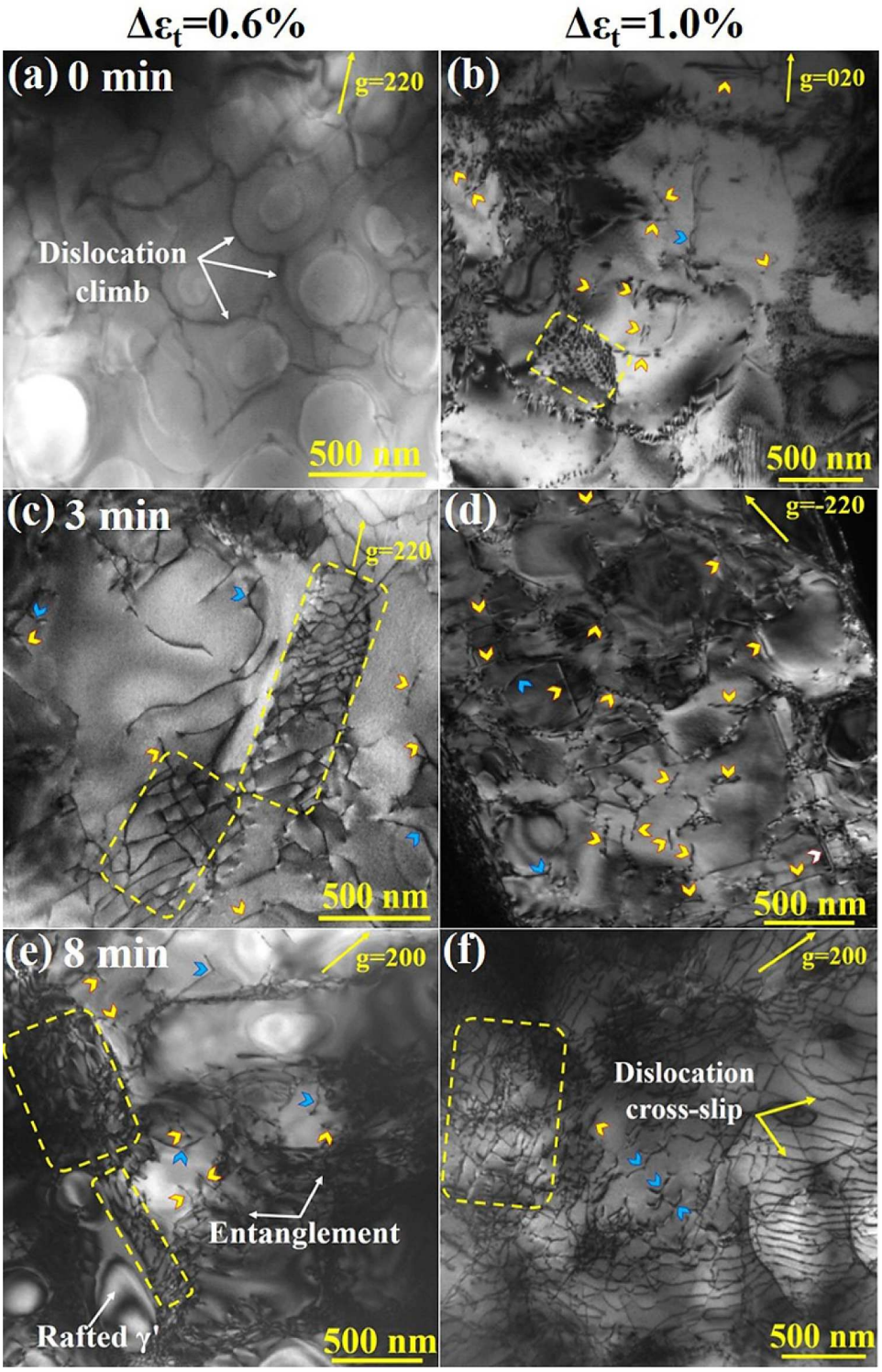

Fig. 13. Dislocation configurations of different total strain ranges at 900 °C. (All dislocations in the figure are taken at Beam//[001]. The g is the operating vector in a two-beam condition. The yellow and blue arrows indicate the straight superdislocations and the curved edge dislocations, respectively. The yellow rectangles represent the dislocation network.).

2017a). Huang et al. once also described that a general relationship between the plastic strain and mobile dislocation density in a dual-phase steel (He et al., 2017). Due to little difference in fracture elongations for various conditions, many straight single superdislocations increase the $\dot{\varepsilon}_{in}$ and accelerate the fracture process, reducing the N_f dramatically. When the dwell time reaches 8 min, there are a small amount of single superdislocations cutting into γ′ phase [Fig. 13(e)]. However, the dislocation networks are formed at the γ/γ′ interface with large amounts of rafted γ′ precipitates, which both impede the movement of subsequent dislocations.

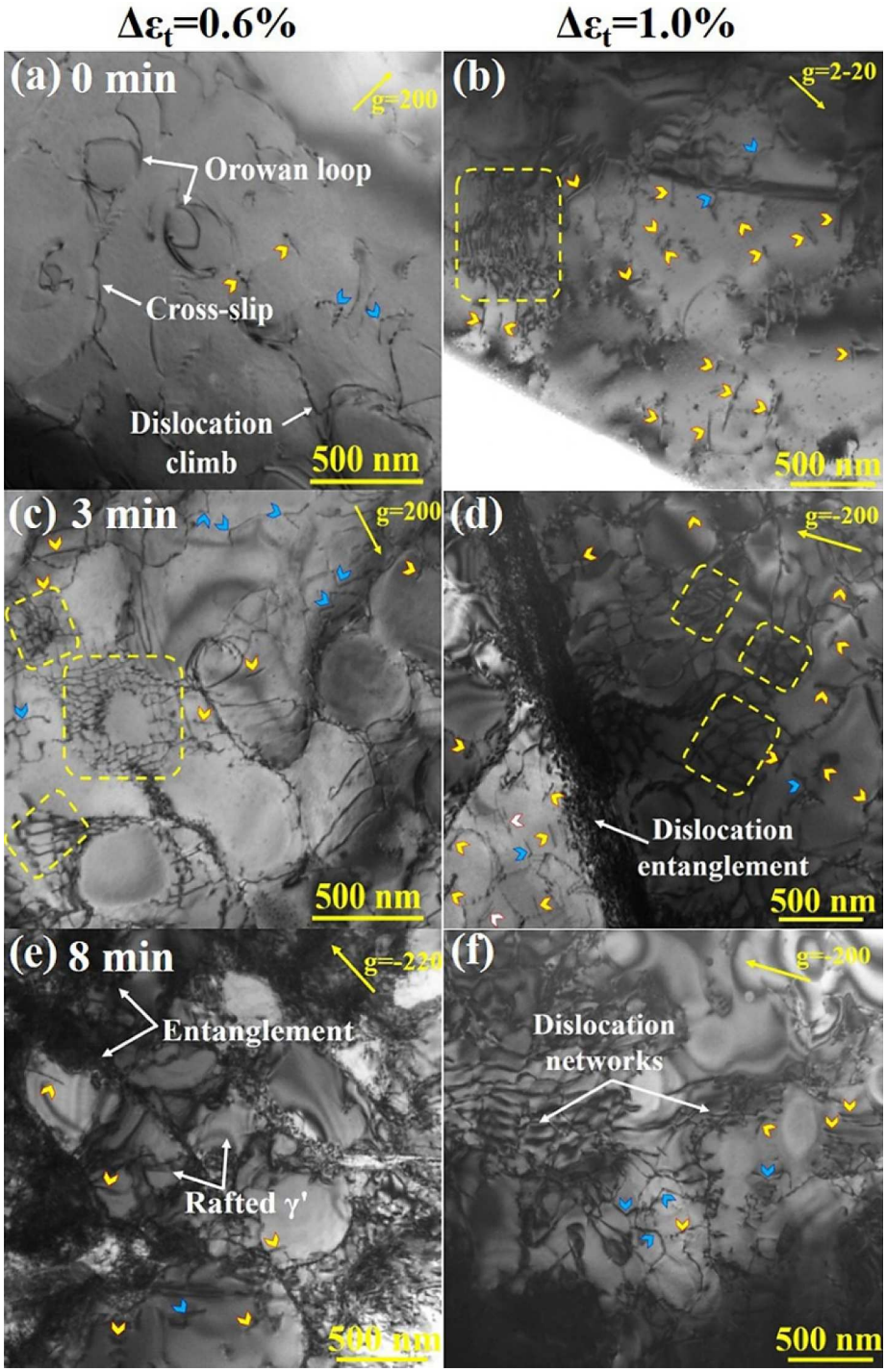

Fig. 14. Another group of dislocation configuration with different total strain ranges at 900 °C. (All dislocations in the figure are taken at Beam// [001]. The g is the operating vector in a two-beam condition. The yellow and blue arrows indicate the straight superdislocations and the curved dislocations, respectively. The yellow rectangles represent the dislocation network.).

Dislocation networks are considered to be useful to strengthen the creep-fatigue properties of materials, reducing the number of mobile dislocations that cut into the γ′ precipitate (Ding et al., 2018c). It corresponds to no further decrease in N_f with 8-minutes dwell time in Fig. 2. It can be deduced that the single straight superdislocations and dislocation networks compete with each other and jointly affect N_f when the dwell time increases. A dynamic equilibrium obtained from the two types of dislocations should be responsible for the saturation-phenomenon formation of cyclic-life.

The dislocation structure at $\Delta\varepsilon_t$ of 1.0% with the dwell time almost shows the same trend as that at $\Delta\varepsilon_t$ of 0.6%. However, there are more single straight superdislocations cutting into γ' phases under the same dwell time as the $\Delta\varepsilon_t$ increases to 1.0% [Figs. 13(b) and (d)]. On the one hand, these features cutting into γ' accelerate the creep-fatigue damage and reduce the fatigue life. On the other hand, it means that the sample suffers the more damage under the condition of no dwell time at the large strain. The application of dwell time causes the alloy to quickly goes into the saturation condition. It can be confirmed from the variation magnitude of single straight dislocations at the dwell time of 0- and 3-minutes. Dislocations at low and high strains correspond to the homogenized and localized damage of cracks and cavities in Section 3.3, respectively. The detailed mechanism of dislocation formation would be given in the discussion part.

4. Discussion

4.1. Mechanism of dislocation movement with different strain ranges

The semi-quantitative analyses of the dislocation type and amount on the N_f are further given in the discussion. Because the TEM images are taken from a highly localized region of the sample. We give another set of TEM pictures to support the creep-fatigue deformation mechanism. The dislocations bypass the γ′ phase mainly in the form of climbing without dwell time at 900 °C and with a $\Delta\varepsilon_t$ of 0.6% [Fig. 14(a)]. Similar phenomena have also been found in fatigue deformation with low strain ranges for the M951G superalloy (Cui et al., 2020). These uniform deformation characteristics result in the long N_f. With a 3-min dwell time [Fig. 14(c)], some superdislocations cut into γ′ when the critical shear stress of γ′ phase is reached. As previously reported, the superdislocation cutting into the γ' phase is one of the important mechanisms in creep, which determines the minimum creep-rate (Müller et al., 2015; Tang et al., 2017b). There are several ways to cut the γ' phase: single superdislocations and coupled superdislocation pairs (Kostka et al., 2007). A type of superdislocation is basically straight, which is also the most common type. Another type of superdislocation is curved, which is formed on different {111} planes that intersect. It is called as Kear-Wilsdorf lock structure, whose dislocation is immovable (Eshelby et al., 1951). It is generally believed that the a<101> superdislocation with higher migration rate in the γ' phase is the main reason for the creep deformation mechanism (Pollock and Argon, 1992). Another form is the a<010> superdislocations with lower mobility (Eggeler and Dlouhy, 1997). The dislocation density and type of these cutting γ' phases will affect the evolution of the superalloy structure.

The yellow arrows in Fig. 14 indicate the single straight superdislocations, which include the type of a<010> superdislocations with lower mobility and type of a/2[101] superdislocations with higher mobility. The straight screw superdislocations of a/2[101] that facilitate to slip on an octahedron in the γ′ phase, whose formation mechanism is revealed in Fig. 15(a). While the blue arrows indicate the curved edge dislocations of a[101] that isn't easy to slip on the (001) plane in the γ′ phase, whose formation mechanism is presented in Fig. 15(b). The greater number of mobile superdislocations increase the $\dot{\varepsilon}_{in}$ and accelerate the fracture process, reducing the N_f dramatically in the case of 3 min. The reason for softening is also attributed to the type of superdislocation with higher mobility and increased density (Tang et al., 2017b). In the creep-fatigue deformation, the shorter dwell time causes the dislocations to rearrange and greatly reduces the dislocation density (Šulák and Obrtlík, 2017), while the longer dwell time promotes the establishment of dislocation networks and increases the dislocation density (ZrníK et al., 2001). When the dwell time reaches 8 min, there are a small amount of single straight superdislocations [Fig. 14(e)]. However, the dislocation networks are formed at the γ/γ′ interface with large

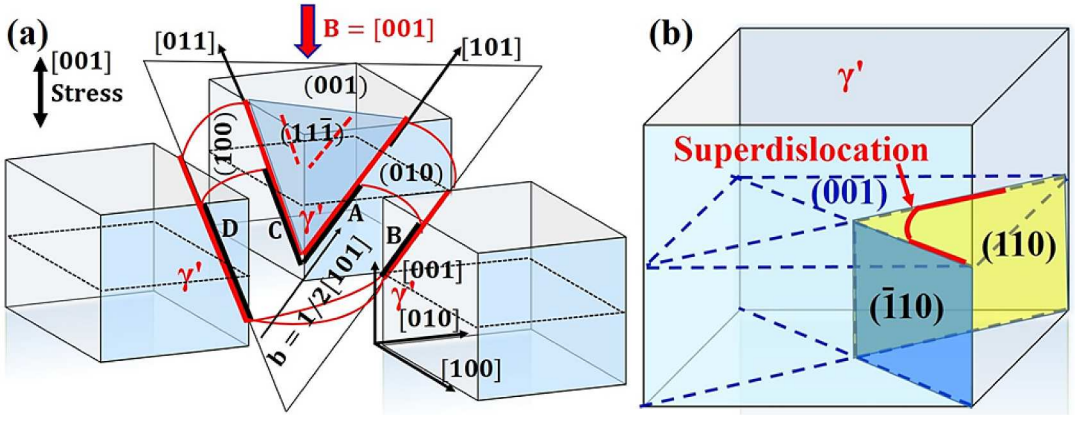

Fig. 15. Diagram of dislocation-deformation mechanisms (a) Screw superdislocation of a/2[101] in the γ' phase. (b) The a[001] edge superdislocations deposited on the (001) plane in the γ' phase are formed by dislocations cross-slipping on different slip planes.

amounts of rafted γ′ precipitates, which both impede the movement of subsequent dislocations. The interface dislocation network (Huang et al., 2014) can prevent the dislocation from bypassing and shearing the γ' precipitates (Shui et al., 2007). It reduced the creep rate, contributing to the enhancement of creep strength of the alloy. Billot (Billot et al., 2010) found that in the stress-controlled creep-fatigue deformation of the cast superalloy Udimet 720 at 700 °C, with the application of dwell time, the dislocation structures were transferred from shearing into γ′ to climbing along with γ′ phase. These dislocation structures correspond to no further decrease in N_f with 8-minutes dwell time in Fig. 2. Since the straight superdislocations accelerate damage of superalloy and the dislocation networks can delay the damage process, the fatigue life is no longer reduced when the two types of dislocations reach a dynamic balance. Then, the N_f saturation state is reached.

There are more screw superdislocations of a/2[101] in the γ' precipitates under the same dwell time as the $\Delta\varepsilon_t$ increases from 0.6% to 1.0% with 0 and 3 min [Figs. 14(b) and (d)]. This trend is because the required APB energy of the superdislocation cut into the γ' phase is constant. The increment of the strain range increases the force at the γ/γ' interface to cut into γ' (Hafez Haghighat et al., 2013). At a higher strain, with the accumulation of the plastic strain, in addition to the superdislocations and the stacking faults cutting the γ' phase, the slip bands with (111)<110> orientations will also be produced (Chu et al., 2008). Thus, the increase in this kind of single superdislocation density makes $\dot{\varepsilon}_{in}$ increase greatly, reducing the N_f. From the above comparison of dislocation characteristics between 0 and 3 min dwell times at the same temperature, the increase of $\Delta\varepsilon_t$ makes the amount of straight single superdislocations in the γ′ phase increase, accelerating the creep-fatigue damage. It takes less time to reach N_f saturation, corresponding to the faster occurrence of the N_f "saturation phenomenon".

4.2. Criterion of cyclic-life "saturation phenomenon"

The deformation mechanism and stress response have been systematically studied above. Then, we strive to find a relationship that could unify these characteristics with the cyclic-life "saturation phenomenon". The parameters are required to describe this trend that the homogenized and localized damage characteristics analyzed above and the difference in energy absorption capacity under different strain ranges. Because the creep-fatigue process belongs to the category of low-cycle-fatigue deformation in the division principle of fatigue life. So the inelastic tensile-strain-energy (ΔU_{in}) and N_f could be expressed by an exponential law similar to the classical Coffin-Manson relationship (Ding et al., 2019):

$$\Delta U_{in} \times \left(2N_f\right)^{-\beta_4} = C_4 \tag{11}$$

where β_4 (without dimension) is the sensitivity index of ΔU_{in} with N_f. It indicates the damage-transition index, suggesting the ability to disperse damage (Liu et al., 2015). The parameter of C_4 (MJ/m^3) represents the energy-absorption capacity of the material (Kong et al., 2019). The area of the hysteresis loop is related to the plastic strain energy of each cycle. After many cycles, the plastic strain energy continues to accumulate. When the number of cycles is large enough to cause the plastic strain energy to increase to a critical value, the material is considered to be fractured. The cyclic failure is an irreversible energy dissipation process. From the energy point of view, materials can withstand various energy absorption capacities at different temperatures (Xiao et al., 1989). Therefore, the energy absorption capacity that the material can withstand under various strain ranges is also different. Thus, the expression could reflect the above-mentioned changes in the creep-fatigue damage mechanism and mechanical response.

The energy-life data with different dwell times of 0 - 8 min under various strain ranges are fitted in Fig. 16(a). We surprisingly found that no matter what strain ranges, the β_4 and C_4 values are reduced with dwell time. It means that the energy-absorption capacity and uniform deformation ability are reduced, corresponding to the formation of the N_f "saturation phenomenon". For the DZ445 superalloy at 900 °C and with the $\Delta\varepsilon_t$ of 0.6%, 1.0%, and 1.6%, β_4 values are 0.64, 0.59, and 0.29; and C_4 values are 43.72, 36.28, and 5.76,

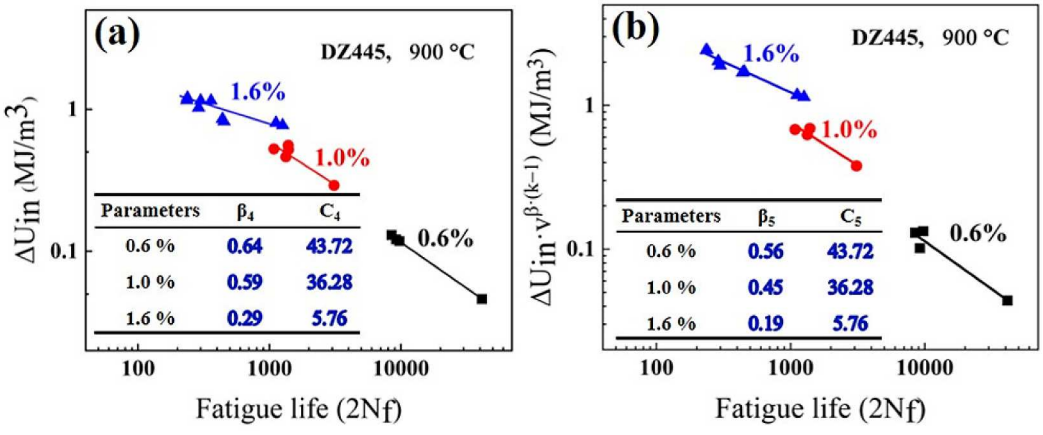

Fig. 16. Relationship between ΔU_{in} and N_f in creep-fatigue deformation with different strain ranges (a) uncorrected-model and (b) frequency correction model.

respectively [Fig. 16(a)], which indicates that the ability to damage dispersion for the DZ445 superalloy is weakened with the increase of strain range. These parameters are traditionally used in energy-based life prediction. But it is the parameter that we used for the first time in this investigation to describe the variation of the "saturation phenomenon" of cycle life. Moreover, these parameters correspond well to the evolution of mechanical responses and damage mechanisms with increasing strain range.

In addition to the traditional Coffin-Manson formula, the creep-fatigue data under different strain ranges were also verified in the frequency-correction energy model. We add the frequency correction term, $V^{(k-1)}$, in Eq. (12) to introduce the influence of oxidation. The corrected data under different strains are fitted in Fig. 16(b). The relationship between the frequency-correction energy (ΔU_{in}) and $2N_f$ is expressed as (Chen et al., 2006),

$$\Delta U_{in}\left(2N_f V^{(k_5-1)}\right)^{\beta_5} = C_5 \tag{12}$$

where k_5 and C_5 are the constants of the material, and V is the cyclic frequency in Hz,

$$V = \frac{1}{T_c + T_h} \tag{13}$$

where T_c and T_h are the dwell time introduced by a single cycle in pure low-cycle fatigue and creep-fatigue deformation, respectively. Comparing Eqs. (11) and 12, the values of C_4 and C_5 are the same. The fitting results in Fig. 16(b) show that both β_5 and C_5 also tend to decrease gradually with the increase of the strain range.

The decreased values of β and C for various models indicate that the ability to damage dispersion for the DZ445 superalloy is weakened and correspond to the localized-deformation mechanism in the case of high strain ranges (Figs. 3-14), indicating that the N_f "saturation phenomenon" appears more easily. Thus, the constants of β and C as the characteristic parameters are first chosen to judge the formation of the N_f "saturation phenomenon" in the creep-fatigue deformation.

4.3. Intrinsic correlation mechanism

The occurrence of the N_f "saturation phenomenon" in creep-fatigue condition is determined by the deformation mechanism, which shows an internal relationship with the mechanical response, fracture characteristics, and saturation criterion. In essence, the stress-relaxation behavior is the process of the Gibbs free-energy reduction (Bober et al., 2017). Under certain test conditions, when the Gibbs-free energy reaches its minimum value, the stress-relaxation curve will appear steady. This trend also corresponds to the dynamic equilibrium process in Section 3.5 of dislocation structures. The decrease in the strain rate during stress relaxation with dwell time is closely related to the growth of plastic voids, which has been described in previous part. As the $\Delta\varepsilon_t$ increases, the relaxation-stress amount increases during the dwell period, indicating that the internal damage of the DZ445 superalloy is aggravated.

In the process of stress relaxation, the elastic strain is gradually transformed into plastic strain. Previous studies have shown that the relationship between the plastic- strain rate and stress is (R.Z. Wang et al., 2016):

$$\dot{\varepsilon}_p = \frac{d\varepsilon_p}{dt} = -\frac{1}{E}\frac{d\sigma}{dt} \tag{14}$$

where $\dot{\varepsilon}_p$ and E represent the plastic strain rate and elastic modulus, respectively.

When the dwell time is initially applied, the plastic-strain relaxation rate is relatively fast, both in the rate of $10^{-4}\ s^{-1}$. In the same total strain range, as the total dwell time increases, the ending of stress relaxation rate gradually decreases. Regardless of the strain range, the $\dot{\varepsilon}_p$ under 8-minutes dwell time is low. These low relaxation rates cause the creep damage, which is reflected in the damage characteristics. Stress relaxation can be regarded as a special creep behavior, and the steady creep rate can be described by the following phenomenological formula (Chen et al., 2014),

Table 4
The stress-relaxation parameters at the characteristic cycle under different total strain ranges at 900 °C. $\dot{\varepsilon}_{init}$, $\dot{\varepsilon}_{end}$, and n_6 are the strain rates at the beginning and ending of the stress relaxation stage and the stress index during the steady stage of the stress relaxation, respectively.

(%)	Dwell time (min)	$\dot{\varepsilon}_{init}$ (s^{-1})	$\dot{\varepsilon}_{end}$ (s^{-1})	n_6
0.6	2	5.94×10^{-4}	5.83×10^{-6}	3.39
0.6	3	1.46×10^{-4}	1.92×10^{-6}	3.58
0.6	5	1.36×10^{-4}	5.92×10^{-7}	4.01
0.6	8	6.72×10^{-5}	4.61×10^{-7}	5.36
1.0	2	5.36×10^{-4}	4.31×10^{-6}	2.34
1.0	3	5.45×10^{-4}	8.62×10^{-6}	3.75
1.0	5	6.25×10^{-4}	7.16×10^{-6}	3.79
1.0	8	8.57×10^{-4}	5.17×10^{-6}	3.96
1.6	2	6.59×10^{-4}	8.47×10^{-6}	11.27
1.6	3	5.44×10^{-4}	5.17×10^{-6}	8.32
1.6	5	7.23×10^{-4}	5.06×10^{-6}	6.32
1.6	8	7.65×10^{-4}	9.29×10^{-7}	6.29

$$\dot{\varepsilon}_p = A\sigma^{n_6} exp\left(-\frac{Q}{RT}\right) \tag{15}$$

where A, Q, R, and T represent the material constant, deformation-activation energy, gas constant (8.314 $Jmol^{-1}$ K^{-1}), and Kelvin temperature, respectively. The stress exponent, " n_6 ", can reflect the deformation mechanism in the process of stress relaxation (Thomas et al., 2006), which can be obtained by the following formula,

$$n_6 = \left(\frac{\partial\ In\ \dot{\varepsilon}_p}{\partial\ In\ \sigma}\right)_T \tag{16}$$

The calculated results of the strain-relaxation rate and stress exponent at the dwell stage under different creep-fatigue loading conditions are listed in Table 4. The change in stress exponent, " n_6 ", corresponds to different deformation mechanisms. As the strain range increases, the value of " n_6 " will continue to increase, corresponding to more superdislocations cutting into the γ′ precipitate (Guo, 2008). This phenomenon has been analyzed in the section of dislocation. It results in the decreased of fatigue life, corresponding to the easier formation of the N_f "saturation phenomenon" at high strain range.

A summary of creep-fatigue mechanical response and damage characteristics under different strain ranges are listed in Table 5. Compared with the cases without the dwell time, the corresponding variation results for those parameters with dwell time as the increased strain range are shown in Fig. 17. The creep-fatigue deformation of the DZ445 superalloy is mainly determined by the ratio of the single straight superdislocations and dislocation networks. The straight superdislocations accelerate damage process, while the dislocation networks show exactly an opposite effect, contrary to the mobile superdislocations. They compete each other all through the deformation process, and the N_f "saturation phenomenon" is formed until they are balanced. The higher strain range results in the greater ratio of mobile superdislocations in the γ′ phase. They give rise to the greater localized-damage characteristic, the worse ability for uniform deformation, the fewer internal voids, the greater hysteresis loop area, and the greater relaxed stress, corresponding to the decreased values of β and C in various models for saturation criterion. In general, the increased strain range results in the decreased time to reach N_f saturation, favoring the formation of N_f "saturation phenomenon".

As we mentioned in this investigation, one feature is that accelerates the material damage. The other feature of dislocation motion is that delays the material damage. Regardless of what strain range, temperature, loading rate, and kind of material, when these two damage modes gradually tend to dynamic equilibrium with the increase of dwell time, the "saturation phenomenon" of cyclic life should be appeared.

In this study, the influence of total strain ranges on the cycle-life "saturation phenomenon" with dwell time was elaborated in detail. This phenomenon of the "saturation phenomenon" has not received widespread attention. There are no reports on the explanation of the behind mechanism and influencing factors in detail before. But its importance in creep-fatigue deformation is similar to the S-N curve in high-cycle fatigue. This investigation has implications for both experiments and services. Due to the consideration of economic benefits, the actual service behavior is usually extrapolated from short-term experiments. Once the saturation limit of N_f is reached, it can eliminate or at least greatly reduce the use of long dwell-time tests. In the creep-fatigue test of a 9Cr-0.5Mo-1.8WV-Nb heat-resistance steel, the reason for not performing the creep-fatigue test for a 60-minutes dwell time is not only because the creep-fatigue test with a long dwell time is costly and time-consuming, but also because the saturated-life of the compression-dwell test is achieved within 10 min (Wang et al., 2018). This phenomenon can also be extended to other alloy systems (Joseph et al., 2020; Zheng et al., 2018). Another important significance of the N_f saturation phenomenon is that when the creep-fatigue cycle-life becomes saturated, the relationship between the rupture time and the dwell time is linear under a certain total strain range. Thus, the rupture time could better characterize the creep-fatigue performance with a long dwell time. It provides the theoretical guidance for the safety design of creep-fatigue in high-temperature components, which is also beneficial to the energy-saving and emission reduction of gas turbines and aero-engines. The proposal of the "saturation phenomenon" of N_f also has the guiding significance for the correction of the creep-fatigue crystal plasticity model.

Table 5
Summary of creep-fatigue mechanical responses and damage characteristics under different strain ranges.

(%)	Dwell time	Saturation rate	Maximum stress	Fracture	Surface crack	Internal cavity	Rafting or not	Dislocation
0.6	Short.	More difficult.	Lower.	Trans-granular.	Short, narrow.	Small.	No.	Orowan loops.
0.6	Long.			Inter-granular.	Long, coarse.	Large.	Yes.	Dislocation networks.
1.0	Short.	Difficult.	Low.	Trans-granular.	Short, narrow.	Small.	No.	Superdislocations cut into γ′.
1.0	Long.			Inter-granular.	Long, coarse.	Large.	Yes.	Dislocation networks.
1.6	Short.	Easy.	High.	Trans-granular.	Long, narrow.	Small.	No.	Slip bands.
1.6	Long.			Inter-granular.	Long, coarse.	Small.	No.	Dislocation networks + stacking faults.

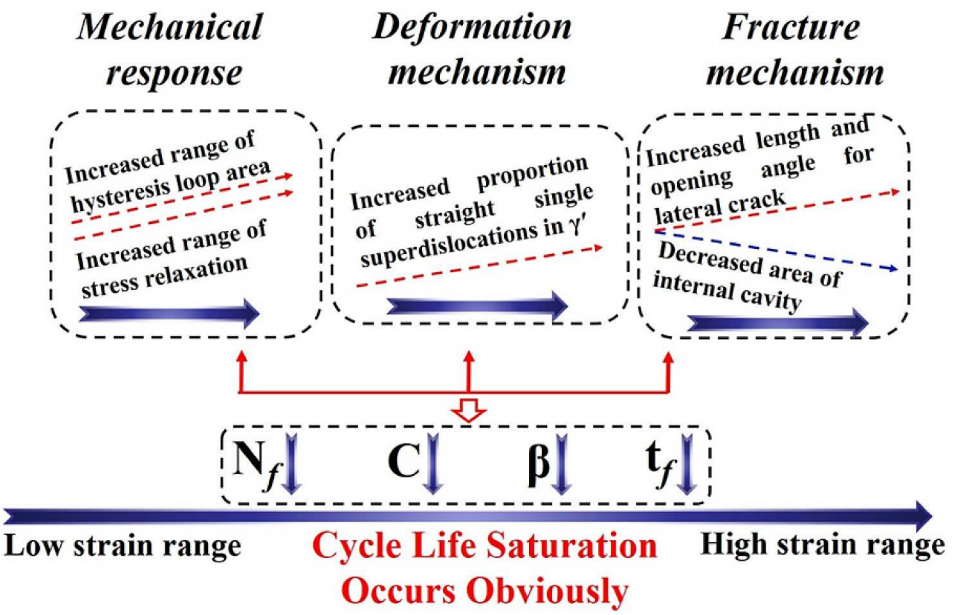

Fig. 17. Summary of the N_f "saturation phenomenon" mechanisms: including the mechanical response and damage mechanism from low to high strain ranges.

4.4. Contribution to the establishment of dislocation-based crystal plasticity models

The crystal plasticity finite element (CPFE) approach has two potential advantages at both the microscopic scale (Chen et al., 2018) and macroscopic scale (Wan et al., 2014) in capturing the grain-level damage evolution of polycrystalline materials. Researchers usually use the cumulative plastic slip, p, (Sweeney et al., 2014) and the cumulative energy dissipation, W, to develop the fatigue life prediction (Korsunsky et al., 2007). Recently, Xu and Prof. Dunne developed an energy-based fatigue prediction index (FIP), defined as energy storage density, to predict the fatigue life (Lu et al., 2020) and explain crack-initiation mechanism (Prastiti et al., 2020), which is related to the plastic slip. The density of statistical storage dislocations (SSD) and geometrically necessary dislocations (GND) is closely related to the model. In addition, Xu (Xu et al., 2021) also quantitatively described the crystal orientation-dependent crack-propagation behavior using the energy storage density. Based on these crystal plasticity models, we strive to give a link between the cyclic-life "saturation phenomenon" and the dislocation-based crystal plasticity model as follow.

Fatigue crack-initiation in pure FCC metals usually originates from the persistent slip band (Essmann et al., 1979). In contrast to the persistent slip band (PSB) mechanism in single crystals (Buque et al., 2001), dislocations in polycrystalline are hindered by grain boundaries (GBs) leading to the stress concentration (Essmann et al., 1981). The Sangid-Maier-Sehitoglu model combines the experimental observations of dislocations, grain boundaries, and twins to predict the fatigue cracks-initiation by PSB (Sangid et al., 2011). However, in the directionally-solidified nickel-based superalloy DZ445 studied in this investigation, the transverse grain boundaries perpendicular to the stress axis are eliminated. Thus, the failure mode for PSB–GB interaction is reduced.

Dyson (Dyson et al., 2009) developed a creep crystal plasticity model for nickel-based single crystal superalloys. The model believes that under creep conditions, dislocations encounter γ′ precipitates and need to slip and climb along the γ/γ′ interface. The total dislocation density ρ is decomposed into the dislocation density ρ^g freely sliding in the γ channel, and the dislocation density ρ^c trapped at the interface of the precipitate and climbing along the interface,

$$\rho = \rho^g + \rho^c \tag{17}$$

where the change rate of ρ^g is the difference between the rate of dislocations released from the interface and the rate of dislocations that are trapped at the γ′ precipitate. The rate at which dislocations are released is the product of the release frequency Γ^e and the trapped dislocations $\frac{2b}{d} f\rho^c$, which are close enough to the corners of the precipitates of size d to escape. If v^g is the sliding velocity in a channel of width w, then the hindered dislocation rate is $\frac{v^g}{w}\rho^g$. Therefore, the rate of change of the sliding dislocation density is:

$$\dot{\rho}^g = \frac{2b}{d} f\rho^c - \frac{v^g}{w}\rho^g \tag{18}$$

The release rate Γ^e depends on the effective diffusivity D_{eff}:

$$\Gamma^e = \frac{D_{eff}}{b^2}\sinh\left(\frac{\tau b^2 w}{kT}\right) \tag{19}$$

It is assumed that the deformation process is governed by the release rate of trapped dislocations at the γ/γ′ interface and that the sliding between precipitate is fast enough, that is, $\frac{v^e}{w} \gg \Gamma^e$. In this case, the final shearing rate is:

$$\dot{\gamma} = 2\rho^m f D_{eff}(1-f)\left(\frac{1}{f^{1/3}}-1\right)\sinh\left(\frac{\tau b^2 w}{kT}\right) \tag{20}$$

where f is the volume fraction of γ' precipitates.

From the above-mentioned dislocation-based crystal plasticity model in nickel-based single crystal superalloys, it can be qualitatively seen that the rate of shearing γ′ precipitate is affected by the difference between the dislocations trapped at the γ/γ′ interface and the hindered dislocations. As shown in Fig. 13 and 14 of TEM images above. With the short dwell time, the mode of short and straight screw superdislocations cutting into the γ' phase are dominated. The dislocations produce plastic deformation by shearing the γ matrix and the γ' precipitate, which aggravates the damage. With the increase of dwell time, the dislocations are eliminated and rearranged, and the number of short and straight screw superdislocations cutting into the γ' phase decreases. While the dislocation network at the γ/γ' interface gradually accumulates. When these dislocation structures reach dynamic equilibrium, a saturated state is reached. Combined with the damage mechanism in the investigation, the results show that with the increase of dwell time, on the one hand, the saturation is reflected in the dislocation structure. On the other hand, the saturation is reflected in the expression of the shearing rate of γ' phase for the dislocation-based crystal plasticity model. The final manifestation is the "saturation phenomenon" of creep-fatigue cyclic life. Meanwhile, a larger strain range corresponds to a higher rate of shearing γ' precipitate. It is hoped that our experimental results can provide guidance for the establishment of the dislocation-based crystal plasticity model of directionally-solidified nickel-based superalloys in the future.

5. Conclusions

The present work reveals the influential mechanism of strain ranges on the cyclic-life saturation during creep-fatigue in nickel-based superalloy DZ445, based on systematical investigation on mechanical response and damage mechanisms under different total strain ranges. The main conclusions are described as follows:

(1) As the dwell time increases, the creep-fatigue cyclic-life becomes saturated, while the rupture time continues to increase. The cyclic-life "saturation phenomenon" appears more easily with increasing strain range.
(2) As the increase of the total strain range, the relative change of the hysteresis loop area with dwell time increase, while the ratio of relaxed stress to the initial value of relaxation during the dwell-period decrease with increasing the dwell time.
(3) With the increase of dwell time, the decrease in the proportion of straight single superdislocations in γ' phase and the increase of the dislocation networks reach dynamic equilibrium, making the cyclic life tend to be saturated. The larger strain range results in the higher ratio of mobile superdislocations cutting into the γ′ phase, resulting in the greater localized-damage characteristic.
(4) At the high total strain range, the fracture mechanism, such as the lateral cracks and internal voids damage, have no enough time to nucleate and grow with the application of dwell time, resulting in the localized-deformation.
(5) The creep-fatigue microscopic deformation-mechanism and macroscopic mechanical-response could be well unified by the various criterion-models of cyclic-life "saturation phenomenon". It also contributes to the establishment of dislocation-based crystal plasticity models for creep-fatigue deformation.

The author team

Biao Ding, Weili Ren*, Yunbo Zhong*, Xiaotan Yuan, Tianxiang Zheng, Zhe Shen*, Yifeng Guo, Qiang Li, Chunmei Liu, Jianchao Peng, Josip Brnic, Yanfei Gao, Peter K. Liaw.

Author statement

B.D. and W.L.R. designed the study. B.D. carried out the main experiments. Y.B.Z. and Z.S. processed the alloy samples. B.D., W.L.R., Y.B.Z., Z.S., P.K.L., Y.F.G., and J.B. analyzed the data and wrote the main draft of the paper. J.C.P. conducted the TEM characterization. All authors discussed the results and commented on the manuscript.

Declaration of Competing Interest

The authors declare that they have no known competing financial interests or personal relationships that could have appeared to influence the work reported in this paper.

Acknowledgements

W.L.R. is grateful for financial supports from the National Science Foundation of China (NSFC) (Grant number 51871142), the Independent Research and Development Project of State Key Laboratory of Advanced Special Steel, Shanghai Key Laboratory of Advanced Ferrometallurgy, Shanghai University (SKLASS 2021-Z08 and Z10), and the Science and Technology Commission of

Shanghai Municipality (No. 19DZ2270200 and 20511107700). B.D. is grateful for the financial support from the fellowship of the China Postdoctoral Science Foundation (2021M692020). Y.B.Z. is grateful for the financial support from the National Key Research and Development Program of China (2018YFB0109404, 2016YFB0300401, and 2016YFB0301401), the National Natural Science Foundation of China (U1732276 and U1860202). P. K. L. very much appreciates the supports from the National Science Foundation (DMR-1611180 and 1809640) with the program directors, Drs. Judith Yang, Gary Shiflet, and Diana Farkas.

References

Billot, T., Villechaise, P., Jouiad, M., Mendez, J., 2010. Creep-fatigue behavior at high temperature of a UDIMET 720 nickel-base superalloy. Int. J. Fatigue 32, 824–829.
Bober, D.B., Lind, J., Mulay, R.P., Rupert, T.J., Kumar, M., 2017. The formation and characterization of large twin related domains. Acta Mater. 129, 500–509.
Brinkman, C., Korth, G., 1973. Heat-to-heat variations in the fatigue and creep-fatigue behavior of AISI type 304 stainless steel at 593 °C. J. Nucl. Mater. 48, 293–306.
Brinkman, C.R., Rittenhouse, P.L., Corwin, W.R., Strizak, J.P., Lystrup, A., DiStefano, J.R., 1976. Application of Hastelloy X in Gas-Cooled Reactor Systems (No. ORNL/TM-5405). Oak Ridge National Lab., Tenn.(USA).
Buque, C., 2001. Persistent slip bands in cyclically deformed nickel polycrystals. Int. J. Fatigue 23, 459–466.
Cao, W., Yang, J., 2021. Unified constitutive modeling of Haynes 230 including cyclic hardening/softening and dynamic strain aging under isothermal low-cycle fatigue and fatigue-creep loads. Int. J. Plast. 138, 102922.
Chen, L., Wu, W., 2006. Creep-fatigue interaction behavior and life prediction of three superalloys. Acta Metall. Sin. (Chinese. Lett.) 42, 952–958.
Chen, G., Zhang, Y., Xu, D.K., Lin, Y.C., Chen, X., 2016. Low cycle fatigue and creep-fatigue interaction behavior of nickel-base superalloy GH4169 at elevated temperature of 650 °C. Mater. Sci. Engin. 655, 175–182.
Chen, J., Jiang, J., Zhen, L., Shao, W., 2014. Stress relaxation behavior of an Al-Zn-Mg-Cu alloy in simulated age-forming process. J. Mater. Process. Technol. 214, 775–783.
Chen, B., Jiang, J., Dunne, F.P., 2018. Is stored energy density the primary meso-scale mechanistic driver for fatigue crack nucleation? Int. J. Plast. 101, 213–229.
Chu, Z., Yu, J., Sun, X., Guan, H., Hu, Z., 2008. High temperature low cycle fatigue behavior of a directionally solidified Ni-base superalloy DZ951. Mater. Sci Engin 488, 389–397.
Conway, J., Berling, J., Stentz, R., 1973. Strain Rate and Holdtime Saturation in Low-Cycle fatigue: Design-parameter plots, Fatigue at Elevated Temperatures. ASTM International.
Cui, L., Liu, J., Peng, R.L., Yu, J., Moverare, J., Sun, X., 2020. Low cycle fatigue behavior and microstructural evolution of nickel-based superalloy M951G at elevated temperatures. Mater. Charact. 163, 110241.
Darling, K., Rajagopalan, M., Komarasamy, M., Bhatia, M., Hornbuckle, B., Mishra, R., Solanki, K., 2016. Extreme creep resistance in a microstructurally stable nanocrystalline alloy. Nature 537, 378.
Ding, B., Ren, W., Deng, K., Li, H., Liang, Y., 2018a. An abnormal increase of fatigue life with dwell time during creep-fatigue deformation for directionally solidified Ni-based superalloy DZ445. High Temp. Mater. Processes (London) 37, 277–284.
Ding, B., Ren, W., Peng, J., Zheng, T., Hou, L., Yu, J., Ren, Z., Zhong, Y., 2019. Damage mechanism and life prediction based on tensile-stress-and compressive-stress-dominated low-cycle fatigue of a directionally solidified Ni-based superalloy DZ445. Mater. Sci. Engin. 742, 478–492.
Ding, B., Ren, W., Peng, J., Zhong, Y., Yu, J., 2018b. Influence of dwell time on the creep–fatigue behavior of a directionally solidified Ni-based superalloy DZ445 at 850 °C. Mater. Sci. Engin. 725, 319–328.
Ding, B., Ren, W., Zhong, Y., Yuan, X., Peng, J., Zheng, T., Shen, Z., Guo, Y., Xuan, W., 2021. Accuracy of the predicting for creep-fatigue cyclic life based on parameters in a characteristic cycle. Eng. Fract. Mech. 255, 107955.
Ding, B., Ren, W., Peng, J., Zhong, Y., Li, F., Yu, J., Ren, Z., 2018c. Revealing the creep-fatigue deformation mechanism for a directionally-solidified Ni-based superalloy DZ445 at 900 °C. Mater. Res. Express. 5, 076513.
Dyson, B.F., 2009. Microstructure based creep constitutive model for precipitation strengthened alloys: theory and application. Mater. Sci. Technol. 25, 213–220.
Essmann, U., Mughrabi, H., 1979. Annihilation of dislocations during tensile and cyclic deformation and limits of dislocation densities. Philos. Mag. A 40, 731–756.
Eggeler, G., Dlouhy, A., 1997. On the formation of< 010>-dislocations in the γ′-phase of superalloy single crystals during high temperature low stress creep. Acta Mater. 45, 4251–4262.
Eshelby, J., Stroh, A.N., 1951. Dislocations in thin plates., 42. The London, Edinburgh, and Dublin Philosophical Magazine and Journal of Science, pp. 1401–1405.
Essmann, U., Gösele, U., Mughrabi, H., 1981. A model of extrusions and intrusions in fatigued metals I. Point-defect production and the growth of extrusions. Philos. Mag. A 44, 405–426.
Fan, Y.N., Shi, H.J., Tokuda, K., 2015a. A generalized hysteresis energy method for fatigue and creep-fatigue life prediction of 316 L (N). Mater. Sci. Engin. 625, 205–212.
Fan, Y.N., Shi, H.J., Qiu, W.H., 2015b. Constitutive modeling of creep behavior in single crystal superalloys: effects of rafting at high temperatures. Mater. Sci. Engin. 644, 225–233.
Fleury, E., Rémy, L., 1994. Behavior of nickel-base superalloy single crystals under thermal-mechanical fatigue. Metall. Mater. Trans. A. 25, 99–109.
Gordon, A., Shenoy, M., Neu, R., McDowell, D., 2006. Fatigue-creep-environment Interactions in a Directionally-Solidified Ni-Base superalloy, Fracture of Nano and Engineering Materials and Structures. Springer, pp. 1243–1244.
Guo, J.T., 2008. Applied Basic Theory of Superalloy Materials Science (I). Science Press.
Hafez, Haghighat, S.M., Eggeler, G., Raabe, D., 2013. Effect of climb on dislocation mechanisms and creep rates in γ′-strengthened Ni base superalloy single crystals: a discrete dislocation dynamics study. Acta Mater. 61, 3709–3723.
Hales, R., 1980. A quantitative metallographic assessment of structural degradation of type 316 stainless steel during creep-fatigue. Fatigue Fract. Eng. Mater. Struct. 3, 339–356.
Halford, G., 1966. The energy required for fatigue(Plastic strain hystersis energy required for fatigue in ferrous and nonferrous metals). J. Mater. 1, 3–18.
He, B., Hu, B., Yen, H., Cheng, G., Wang, Z., Luo, H., Huang, M.X., 2017. High dislocation density–induced large ductility in deformed and partitioned steels. Science 357, 1029–1032.
Hirth, JohnPrice, 1983. Theory of Dislocations, 2nd ed. Wiley.
Hormozi, R., Biglari, F., Nikbin, K., 2015. Experimental and numerical creep-fatigue study of Type 316 stainless steel failure under high temperature LCF loading condition with different hold time. Eng. Fract. Mech. 141, 19–43.
Huang, M., Cheng, Z., Xiong, J., Li, J., Hu, J., Liu, Z., Zhu, J., 2014. Coupling between Re segregation and γ/γ′ interfacial dislocations during high-temperature, low-stress creep of a nickel-based single-crystal superalloy. Acta Mater. 76, 294–305.
Joseph, S., Joseph, K., Lindley, T.C., Dye, D., 2020. The role of dwell hold on the dislocation mechanisms of fatigue in a near alpha titanium alloy. Int. J. Plast. 131, 102743.
Kim, Y.K., Kim, D., Kim, H.K., Oh, C.S., Lee, B., 2016. An intermediate temperature creep model for Ni-based superalloys. Int. J. Plast. 79, 153–175.
Kirka, M.M., Brindley, K.A., Neu, R.W., Antolovich, S.D., Shinde, S.R., 2015. Influence of coarsened and rafted microstructures on the thermomechanical fatigue of a Ni-base superalloy. Int. J. Fatigue 81, 191–201.
Kong, W.W., Yuan, C., Zhang, B.N., Qin, H.Y., Zhao, G.P., 2019. Investigation on low-cycle fatigue behaviors of wrought superalloy GH4742 at room-temperature and 700 °C. Mater. Sci. Engin. 751, 226–236.
Kostka, A., Mälzer, G., Eggeler, G., Dlouhy, A., Reese, S., Mack, T., 2007. L12-phase cutting during high temperature and low stress creep of a Re-containing Ni-base single crystal superalloy. J. Mater. Sci. 42, 3951–3957.

Kruzic, J.J., 2009. Predicting fatigue failures. Science 325, 156–158.
Korsunsky, A.M., Dini, D., Dunne, F.P., 2007. Comparative assessment of dissipated energy and other fatigue criteria. Int. J. Fatigue 29, 1990–1995.
León-Cázares, F., Monni, F., Jackson, T., Galindo-Nava, E., Rae, C., 2020a. Stress response and microstructural evolution of nickel-based superalloys during low cycle fatigue: physics-based modelling of cyclic hardening and softening. Int. J. Plast. 128, 102682.
León-Cázares, F.D., Schlütter, R., Jackson, T., Galindo-Nava, E.I., Rae, C., 2020b. A multiscale study on the morphology and evolution of slip bands in a nickel-based superalloy during low cycle fatigue. Acta Mater. 182, 47–59.
Liu, G., Winwood, S., Rhodes, K., 2020. The effects of grain size, dendritic structure and crystallographic orientation on fatigue crack propagation in IN713C nickel-based superalloy. Int. J. Plast. 125, 150–168.
Liu, R., Zhang, Z., Zhang, P., Zhang, Z., 2015. Extremely-low-cycle fatigue behaviors of Cu and Cu–Al alloys: damage mechanisms and life prediction. Acta Mater. 83, 341–356.
Lord, D.C., Coffin, L.F., 1973. Low cycle fatigue hold time behavior of cast Rene 80. Metall. Trans. 4, 1647–1654.
Lu, X., Dunne, F.P., Xu, Y., 2020. A crystal plasticity investigation of slip system interaction, GND density and stored energy in non-proportional fatigue in Nickel-based superalloy. Int. J. Fatigue 139, 105782.
McDaniels, R., Chen, L., Steward, R., Liaw, P., Buchanan, R., White, S., Liaw, K., Klarstrom, D.J.M.S., A, E., 2011. The strain-controlled fatigue behavior and modeling of Haynes® HASTELLOY® C-2000® superalloy 528, 3952–3960.
Meurer, H.P., Gnirss, G.K.H., Mergler, W., Raule, G., Schuster, H., Ullrich, G., 1984. Investigations on the fatigue behavior of high-temperature alloys for high-temperature gas-cooled reactor components. Nucl. Technol. 66, 315–323.
Miao, J., Pollock, T.M., 2009. Crystallographic fatigue crack initiation in nickel-based superalloy René 88DT at elevated temperature. Acta Mater. 57, 5964–5974.
Müller, J., Eggeler, G., Spiecker, E., 2015. On the identification of superdislocations in the γ′-phase of single-crystal Ni-base superalloys–An application of the LACBED method to complex microstructures. Acta Mater. 87, 34–44.
Nagae, Y., 2013. Evaluation of creep-fatigue life based on fracture energy for modified 9Cr–1Mo steel. Mater. Sci. Engin. 560, 752–758.
Novelo, O., González, G., Characterization, G.A., 2008. Characterization of precipitation in Al-Mg-Cu alloys by X-ray diffraction peak broadening analysis. Mater. Charact. 59, 773–780.
Ostergren, W.J., 1976. A damage function and associated failure equations for predicting hold time and frequency effects in elevated temperature, low cycle fatigue. J. Test. Eval. 4, 327–339.
Pollock, T.M., Argon, A.S., 1992. Creep resistance of CMSX-3 nickel base superalloy single crystals. Acta Metall. Mater. 40, 1–30.
Porter, T., Findley, K., Kaufman, M., Wright, R., 2019. Assessment of creep-fatigue behavior, deformation mechanisms, and microstructural evolution of alloy 709 under accelerated conditions. Int. J. Fatigue 124, 205–216.
Prastiti, N.G., Xu, Y., Balint, D.S., 2020. Discrete dislocation, crystal plasticity and experimental studies of fatigue crack nucleation in single-crystal nickel. Int. J. Plast. 126, 102615.
Reed, R., Cox, D., C., 2007. Damage accumulation during creep deformation of a single crystal superalloy at 1150 °C. Mater. Sci. Engin. 448, 88–96.
Reed, R., 2006. The Superalloys. Cambridge University Press.
Rodas, E.A.E., Neu, R.W., 2018. Crystal viscoplasticity model for the creep-fatigue interactions in single-crystal Ni-base superalloy CMSX-8. Int. J. Plast. 100, 14–33.
Rodriguez, P., Rao, K.B.S., 1993. Nucleation and growth of cracks and cavities under creep-fatigue interaction. Prog. Mater Sci. 37, 403–480.
Shi, D., Dong, C., Yang, X., Sun, Y., Wang, J., Liu, J., 2013. Creep and fatigue lifetime analysis of directionally solidified superalloy and its brazed joints based on continuum damage mechanics at elevated temperature. Mater. Des. 45, 643–652.
Shi, D., Liu, J., Yang, X., Qi, H., Wang, J., 2010a. Experimental investigation on low cycle fatigue and creep–fatigue interaction of DZ125 in different dwell time at elevated temperatures. Mater. Sci. Engin. 528, 233–238.
Shui, L., Jin, T., Tian, S., Hu, Z., 2007. Influence of precipitate morphology on tensile creep of a single crystal nickel-base superalloy. Mater. Sci. Eng., A. 454, 461–466.
Smith, T.M., Esser, B.D., Antolin, N., Carlsson, A., Williams, R.E.A., Wessman, A., Hanlon, T., Fraser, H.L., Windl, W., Mccomb, D.W., 2016. Phase transformation strengthening of high-temperature superalloys. Nat. Commun. 7, 13434.
Stinville, J.C., Martin, E., Karadge, M., Ismonov, S., Soare, M., Hanlon, T., Sundaram, S., Echlin, M.L.P., Callahan, P.G., Lenthe, W.C., 2018. Fatigue deformation in a polycrystalline nickel base superalloy at intermediate and high temperature: competing failure modes. Acta Mater. 152, 16–33.
Šulák, I., Obrtlík, K., 2017. Effect of tensile dwell on high-temperature low-cycle fatigue and fracture behaviour of cast superalloy MAR-M247. Eng. Fract. Mech. 185, 92–100.
Sweeney, C.A., O'Brien, B., Dunne, F.P., et al., 2014. Strain-gradient modelling of grain size effects on fatigue of CoCr alloy. Acta Mater. 78, 341–353.
Sangid, M.D., Maier, H.J., Sehitoglu, H., 2011. The role of grain boundaries on fatigue crack initiation–an energy approach. Int. J. Plast. 27, 801–821.
Takahashi, Y., 2008. Study on creep-fatigue evaluation procedures for high-chromium steels—Part I: test results and life prediction based on measured stress relaxation. Int. J. Press. Vessels Pip. 85, 406–422.
Tang, Y., Huang, M., Xiong, J., Li, J., Zhu, J., 2017. Evolution of superdislocation structures during tertiary creep of a nickel-based single-crystal superalloy at high temperature and low stress. Acta Mater. 126, 336–345.
Thomas, A., El-Wahabi, M., Cabrera, J., Prado, J., 2006. High temperature deformation of Inconel 718. J. Mater. Process. Technol. 177, 469–472.
Tian, Y., Yu, D., Zhao, Z., Chen, G., Chen, X., 2016. Low cycle fatigue and creep-fatigue interaction behaviour of 2.25 Cr1MoV steel at elevated temperature. Mater. High Temp. 33, 75–84.
Wang, R.Z., Zhang, X.C., Tu, S.T., Zhu, S.P., Zhang, C.C., 2016a. A modified strain energy density exhaustion model for creep-fatigue life prediction. Int. J. Fatigue 90, 12–22.
Wang, R.Z., Zhang, X.C., Gong, J.G., Zhu, X.M., Tu, S.T., Zhang, C.C., 2017. Creep-fatigue life prediction and interaction diagram in nickel-based GH4169 superalloy at 650 C based on cycle-by-cycle concept. Int. J. Fatigue 97, 114–123.
Van Sluytman, J.S., Pollock, T.M., 2012. Optimal precipitate shapes in nickel-base γ–γ′ alloys. Acta Mater. 60, 1771–1783.
Wan, V.V.C., MacLachlan, D.W., Dunne, F.P., 2014. A stored energy criterion for fatigue crack nucleation in polycrystals. Int. J. Fatigue 68, 90–102.
Wareing, J., 1981. Creep-fatigue behaviour of four casts of type 316 srainless steel. Fat. Fract. Engin. Mater. Struc. 4, 131–145.
Wu, X., Makineni, S.K., Liebscher, C.H., Dehm, G., Gault, B., 2020. Unveiling the *Re* effect in Ni-based single crystal superalloys. Nat. Commun. 11, 1–13.
Wang, X., Zhang, W., Gong, J., Wahab, M.A., 2018. Low cycle fatigue and creep fatigue interaction behavior of 9Cr-0.5 Mo-1.8 WV-Nb heat-resistant steel at high temperature. J. Nucl. Mater. 505, 73–84.
Xiao, T., De, W., Hao, X., 1989. Investigation of cyclic hysteresis energy in fatigue failure process. Int. J. Fatigue. 11, 353–359.
Xu, Y., 2021. A non-local methodology for geometrically necessary dislocations and application to crack tips. Int. J. Plast. 140, 102970.
Yablinsky, C.A., Flores, K.M., Mills, M.J., Williams, J.C., Rigney, J., 2008. Fatigue behavior in monocrystalline Ni-based superalloys for blade Applications. Superalloys.
Zhang, J.S., 2007. Deformation and Fracture of Materials At High Temperature. Science Press.
Zhang, Q., Zhang, Z., 2011. In situ observations on creep fatigue fracture behavior of Sn–4Ag/Cu solder joints. Acta Mater. 59, 6017–6028.
Zhang, X., Tu, S., Xuan, F., 2014. Creep-fatigue endurance of 304 stainless steels. Theor. Appl. Fract. Mech. 71, 51–66.
Zheng, Z., Stapleton, A., Fox, K., 2018. Understanding thermal alleviation in cold dwell fatigue in titanium alloys. Int. J. Plast. 111, 234–252.
ZrníK, J., Semeňák, J., Vrchovinský, V., Wangyao, P., 2001. Influence of hold period on creep-fatigue deformation behaviour of nickel base superalloy. Mater. Sci. Engin. A 319, 637–642.
Zhu, S.P., Lei, Q., Huang, H.Z., Yang, Y.J., Peng, W., 2017. Mean stress effect correction in strain energy-based fatigue life prediction of metals. Int. J. Damage Mech. 26 (8), 1219–1241.